1   **Phloem loading via the abaxial bundle sheath cells in maize leaves**

2

3

4   **Margaret Bezrutczyk[1], Nora R. Zöllner[1], Colin P. S. Kruse[2], Thomas Hartwig[1], Tobias**

5   **Lautwein[3], Karl Köhrer[3], Wolf B. Frommer[1,4,*] and Ji-Yun Kim[1]**

6

7

8   **AFFILIATIONS**

9   [1] Institute for Molecular Physiology, Heinrich-Heine-University Düsseldorf, Düsseldorf 40225,

10   Germany

11   [2] Los Alamos National Laboratory, Los Alamos, New Mexico, USA, 87545

12   [3] Biological and Medical Research Center (BMFZ), Genomics and Transcriptomics Laboratory

13   (GTL), Medical Faculty, Heinrich Heine University Düsseldorf, Düsseldorf, Germany

14   [4] Institute of Transformative Bio-Molecules (WPI-ITbM), Nagoya University, Chikusa, Nagoya

15   464-8601, Japan

16

17   * Correspondence: frommew@hhu.de

18

19 **ABSTRACT**

20 Leaves are asymmetric, with differential functionalization of abaxial and adaxial tissues. The

21 bundle sheath (BS) surrounding the vasculature of the C3 crop barley is dorsoventrally

22 differentiated into three domains: adaxial structural, lateral S-type, and abaxial L-type. S-type cells

23 seem to transfer assimilates towards the phloem. Here we used single-cell RNA sequencing to

24 investigate BS differentiation in C4 maize. Abaxial BS ([ab]BS) cells of rank-2 intermediate veins

25 specifically expressed three SWEET sucrose uniporters (*SWEET13a, b,* and *c*) and UmamiT amino

26 acid efflux transporters. *SWEET13a, b, c* were also identified in the phloem parenchyma (PP). Thus

27 maize acquired a unique mechanism for phloem loading in which [ab]BS cells provide the main

28 pathway for apoplasmic sucrose transfer towards the phloem. This pathway predominates in veins

29 responsible for phloem loading (rank-2 intermediate), while rank-1 intermediate and major veins

30 export sucrose from the phloem parenchyma (PP) adjacent to the sieve element companion cell

31 (SE/CC) complex, as in Arabidopsis. We surmise that [ab]BS identity is subject to dorsoventral

32 patterning and has components of PP identity. These observations provide first insights into the

33 unique transport-specific properties of [ab]BS cells and support for a modification to the canonical

34 phloem loading pathway of maize, which may be generalizable to other C4 monocots.

35

36

37

38 **KEYWORDS**

39 Single cell sequencing, *Zea mays* L., SWEET, SUT, sucrose, transporter, UmamiT, amino acid

40 transporter

41

42   **INTRODUCTION**

43   Leaves are typically asymmetric: there are often differences in the relative stomatal and trichome

44   densities and cuticle properties between the abaxial and adaxial leaf surfaces. While maize leaves

45   are amphistomatic, asymmetry remains apparent, with bulliform cells only on the adaxial side and

46   a conjoint, collateral and closed-type vasculature, with adaxial xylem and abaxial phloem.

47   Dorsoventral patterning in maize leaf is initiated in the shoot apical meristem at the earliest stages

48   of leaf primordia development by expression of *RGD2* (*Ragged seedling2*) (Henderson et al., 2006)

49   and adaxial expression of *RLD1* (*Rolled leaf1*), which is conferred by miRNA166-mediated *RLD1*

50   transcript cleavage on the abaxial side (Juarez et al., 2004b, 2004a). This pattern is maintained

51   throughout development by specific localization of numerous transcription factors, including the

52   abaxial expression of *KANADI* (Candela et al., 2008). Bundle sheath cells (BSCs) of maize are not

53   known to be functionally differentiated. In barley leaves, the BSCs are anatomically distinct:

54   abaxial side "L-type" BSC have large chloroplasts, while "S-type" BSCs, with small chloroplasts,

55   surround the rest of the mestome sheath. It was proposed that the S-type cells may be specialized

56   for photoassimilate transport, based on the rapid disappearance of starch after the light period and

57   the abundant plasmodesmatal connections between S-type cells, mestome sheath, and phloem

58   (Williams et al., 1989). In maize, the two abaxial BSCs ([ab]BSCs) are typically smaller compared to

59   the medial BSCs. *In situ* hybridization and immunolocalization had shown that Rubisco, the

60   glutamine synthetase isoform GS1-4 (*GLN3*), and malic enzyme localized specifically to BS, with

61   transcripts and proteins equally represented in all BSCs (Langdale et al., 1988a; Martin et al., 2006).

62   Here we used single cell RNA sequencing (scRNA-seq) to test whether the BS of the C4 plant

63   maize is uniform or also shows a dorsoventral differentiation of its cells, as found in barley. The

64   analysis identified mesophyll- and bundle sheath-specific transcripts and found that the BS could

65   be subclustered into two groups, one specifically expressing a variety of genes including SWEET13

66   sucrose transporters, UmamiT and AAP amino acid transporters, as well as several transcription

3

67   factors. *In situ* hybridization and analysis of translational GUS fusions demonstrated that the

68   subclustering was due to dorsoventral patterning, as evidenced by the finding that the three

69   SWEET13 paralogs were specifically expressed in [ab]BS. These findings not only show that the

70   maize leaf BS is functionally differentiated, but also identify a unique pathway for apoplasmic

71   phloem loading in a C4 plant. In addition, the three SWEET13s were also present in cells that most

72   likely represent the phloem parenchyma, similar to the profiles of their Arabidopsis orthologs

73   AtSWEET11, 12, and 13. Maize [ab]BS thus appears to use a combination of dorsoventral patterning

74   and PP identity to drive sucrose into the apoplasm of the phloem.

4

75   **RESULTS**

76   **mRNA patterns of specific cell types in maize leaves**

77   To determine whether maize leaves contain multiple BSC types, we performed single-cell

78   sequencing on protoplasts isolated from maize leaves. We first established a protocol for protoplast

79   release. To minimize the possibility of a developmental gradient across cells, fully differentiated

80   tissue was harvested from the distal portion of leaf 2 of late V2 stage plants (first and second leaf

81   collar exposed) (Li et al., 2010) (Fig. 1a). Standard leaf protoplasting protocols leave intact bundle

82   sheath 'strands,' consisting of BSCs and the vasculature (Kanai and Edwards, 1973; Langdale et

83   al., 1989). In a parallel study, we were able to optimize protoplasting of Arabidopsis leaves to

84   increase the yield of vascular cell types (Kim et al., 2020). We compared published protocols and

85   varied parameters such as incubation time, enzyme concentration, enzyme blend, and preincubation

86   in L-cysteine (Ortiz-Ramírez et al., 2018). Efficiency of the release of putative vascular cells was

87   monitored using qRT-PCR with cell-type specific markers, under the assumption that the *SWEET13*

88   paralogs, analogous to their Arabidopsis orthologs, would be specific to phloem parenchyma.

89   Although none of the protocols were able to yield efficient release of putative vascular cells, we

90   obtained apparent release of both BSCs and vascular cells with Protocol 4 (Supplementary Fig. 1).

91   An estimated 7,000 protoplasts were pipetted into a 10x Chromium microfluidic chip, and single

92   cell cDNA libraries were generated and sequenced. Gel bead-specific barcodes were used to

93   identify mRNAs present in specific cells. After filtering the dataset to select for healthy cells, 4,035

94   cells with an average of 4,874 mRNA molecules per cell were analyzed. Unsupervised clustering

95   was performed using Seurat (Butler et al., 2018) to determine the relationship between mRNA

96   expression profiles in PCA space, ultimately represented in a two-dimensional UMAP plot (Fig.

97   1b). Cell identities were assigned to the clusters based on established marker genes for different

98   cell types (Supplementary Table 1). We obtained six clusters, five of which formed a large

99   supercluster that all had mesophyll identities, and one separate cluster corresponding to bundle

5

100   sheath identity (Fig. 1c). The distribution of marker genes was consistent with the roles of

101   mesophyll and BS cells in C4 photosynthesis (Supplementary Fig. 2, Supplementary Table 2). The

102   ratio of mesophyll to BSC was ~75:1, indicating a low efficiency of BSC retrieval. To our surprise,

103   no vascular cells were recovered. The BS cluster was further divided into two subclusters, the

104   "upper" and "lower" subclusters, which later were assigned as abaxial (^{ab}BS) and adaxial (^{ad}BS)

105   bundle sheath cells (Fig. 1d, Fig. 2) (see below).

106   **Mesophyll and bundle sheath clusters show canonical expression of C4 photosynthesis genes**

107   Unsupervised clustering resulted in five clusters of mesophyll cells based on the presence of

108   canonical C4 marker genes. At first sight the presence of five clusters was surprising. Cluster MS1

109   included most mesophyll cells and likely represents the core mesophyll. MS1 was enriched in

110   photosynthetic processes. MS2 was enriched for the GO terms triose phosphate transport

111   (GO:0035436; GO:0015717), nucleic acid metabolic process, immune system process

112   (GO:0002376) and RNA metabolic process (GO:0016070) (Supplementary Table 1, 3). MS3 and

113   MS4 contained high levels of rRNA transcripts. rRNA was not removed before sample preparation

114   nor were cells with higher rRNA transcript levels, as rRNA levels can vary between cells. Whether

115   these rRNA-enriched clusters represent biologically relevant cell populations in the leaf or are due

116   to artifacts was not further evaluated. An additional subcluster, MS5, had an apparent mesophyll

117   identity, but was clearly separated from the other mesophyll clusters. The main determinants for

118   this separate clustering were iron/metal-related processes (Supplementary Text). Due to the focus

119   on BSCs, localization and biological relevance of MS5 was not characterized further. Our

120   clustering data are supported by the presence of transcripts for the glutamine synthetase

121   *GLN4* (corresponding to *gln1-3* and protein GS1-3) in the MS1-4 cells, consistent with previous *in*

122   *situ* and immunolocalization data that detected glutamine synthetase specifically in the mesophyll

123   (Supplementary Fig. 3) (Martin et al., 2006).

6

124   It may be interesting to explore further whether the subclustering of mesophyll cells represents

125   developmental trajectories or physiological differences. We did not identify an obvious pattern that

126   could be attributed to, for example, dorsoventral patterning due to developmental gradients or due

127   to changes in light properties as it passes through the leaf. Similar observations regarding the

128   presence of multiple mesophyll clusters were made for scRNA-seq analyses of Arabidopsis leaves,

129   however, it was not possible to assign palisade and spongy parenchyma to any of the mesophyll

130   clusters (Kim et al., 2020).

131   **Both subsets of bundle sheath cells express canonical C4 photosynthesis genes**

132   In maize, photosynthesis is partitioned between the mesophyll and bundle sheath cells (Li et al.,

133   2010; Chang et al., 2012; Friso et al., 2010), allowing us to differentiate between these cell

134   populations based on their mRNA profiles. Maize leaves utilize an NADP-ME-dependent C4

135   pathway, and mesophyll cells and bundle sheath cells must exchange intermediate species via

136   plasmodesmata, with specific enzymes highly upregulated in one cell type or the other. To identify

137   the clusters, we selected several key marker genes that are known to be differentially expressed in

138   either mesophyll or bundle sheath.

139   Most of the genes involved in primary carbon metabolism, which showed significant differential

140   expression in the 2010 proteomics survey of MS and BS chloroplasts (Friso et al., 2010), were

141   expressed in the expected cell types in our dataset (Supplementary Fig. 2, Supplementary Table 1,

142   2), except for the predicted chloroplast envelope transporter *TPT* and the Calvin cycle enzyme

143   *PGK2*, which were both expressed nearly equally in both MS and BS clusters. For example,

144   transcripts of pyruvate orthophosphate dikinase 2 (*PDK2*) were almost exclusively found in BSCs,

145   while *PDK1* transcript levels were high in mesophyll (Supplementary Fig. 2, Supplementary Table

146   1, 2), in agreement with both proteomics data (Friso et al., 2010) and their corresponding

147   contributions to C4 photosynthesis (Chastain et al., 2017). All cells in the BSC subcluster showed

148   high and specific expression of the canonical C4 photosynthesis-related genes that function in the

149   BSCs, including *RBCS*, *ME1*, and *PCK1* (Supplementary Fig. 2, Supplementary Table 2). The

150   Rubisco small chain mRNAs (*RBCS1*, *RBCS2*) were equally distributed in both abaxial and adaxial

151   BS subclusters (Fig. 1). The bundle sheath-specific glutamine synthetase *GLN3* (corresponding to

152   gene *gln1-4* and protein GS1-4) was found in both BS subclusters, consistent with *in situ* and

153   immunolocalization data that showed no evidence for a specific pattern for GS1-4 in the BS

154   (Supplementary Fig. 3) (Martin et al., 2006).

Abaxial BS cluster is enriched for genes encoding transport proteins

156   The two BS cell subclusters (Fig. 1d) could either represent developmental trajectories along the

157   leaf axis, BS cells from the three different vein classes (major vein or rank-l or rank-2 intermediate

158   veins), different physiological states, or dorsoventral patterning. While the majority of mRNAs

159   corresponded to BS identity, only 5 genes appeared specific to ^{ad}BS (the "lower subcluster") and

160   39 to ^{ab}BS (the "upper" subcluster) (Table 1). Surprisingly, among the genes with the highest

161   difference between the two BS subclusters were the three *SWEET13a*, *b*, and *c* paralogs. SWEETs

162   are uniporters, and maize SWEET13a, b and c function as sucrose transporters.

163   Similar to their orthologs AtSWEET11 and 12 from Arabidopsis, in maize leaves SWEET13a, b,

164   and c are critical for phloem loading of sucrose (Bezrutczyk et al., 2018), though it remained

165   unknown if the maize SWEET13s were co-expressed in the same cells and in which cell types they

166   function. All three *SWEET13* paralogs were present in BSCs in maize, while the Arabidopsis

167   orthologs *AtSWEET11*, *12* and *13* are specifically expressed in PP (Kim et al., 2020). This

168   observation is consistent with the qRT-PCR results performed during the optimization of the

169   protoplast protocol, which detected *SWEET13* transcripts, but no vascular cells were recovered by

170   scRNA-seq. The "upper" BS subcluster, ^{ab}BS, showed a striking enrichment for transport proteins,

171   with 9 of 39 ^{ab}BS-specific genes involved in transport (Table 1). Importantly, this included not only

172   *SWEET13a*, *b*, and *c*, but also an STP hexose transporter (STP3), the amino acid efflux transporter

173   *UmamiTT21a* (Supplementary Fig. 4), two members of the H^+/amino acid symporter family,

8

174   *AAP56* and *AAP45* (Deng, 2014), a member of the nitrate peptide transport family, and the H$^+$-

175   ATPase AHA3 (Table 1). Notably, in Arabidopsis, transcripts for the closest Arabidopsis homolog

176   of Zm*UmamiT21a*, *AtUmamiT21*, were enriched in PP (Fig. 3) and co-expressed with *AtSWEET11*

177   and *12* in Arabidopsis. On the basis of the presence of SWEETs, UmamiT21 and other [ab]BS-

178   enriched candidates, one may speculate that the transcription factors that in Arabidopsis are

179   involved in PP identity have been recruited in maize to [ab]BS to drive the unique set of genes

180   expressed in [ab]BS. *DOF3* (*DNA binding with one finger3*) is a transcription factor implicated in the

181   control of SWEET gene expression in rice (Wu et al., 2018) which shows [ab]BS-specific expression

182   in this dataset; two other transcription factors, *bZIP4* (*ABA-insensitive 5-like protein*) and *MYB25*

183   (just below p-value cutoff), were enriched in [ab]BS. While [ab]BS-enriched, *bZIP* and *MYB25* were

184   not BS-specific, but only sparsely expressed in mesophyll cells (Supplementary Figure 3).

185   Other BSC-specific genes such as *RBCS1* showed equal transcript distribution across all BS cells,

186   excluding the possibility of an artefact, e.g., a gradient of cells differing in UMI counts. This

187   included *UmamiT20a*, which was BS-enriched but equally expressed across both BS subclusters.

188   The lack of specificity of many genes for subsets of BSC is consistent with published data from *in*

189   *situ* hybridization and immunolocalization of *RBCS1* and glutamine synthetase, both of which did

190   not show dorsoventral patterning (Langdale et al., 1988a; Martin et al., 2006; Langdale et al.,

191   1988b).

192   To test the hypothesis that the two BS subclusters may represent spatially discrete BSC populations,

193   *in situ* hybridization was used to localize the mRNAs of the *SWEET13a, b,* and *c* genes (Fig. 2b-f,

194   Supplementary Fig. 5). Notably, transcripts of all three *SWEET13* genes were specifically detected

195   in the two abaxial bundle sheath cells ([ab]BSCs) adjacent to the phloem. Additionally, *SWEET13a,*

196   *b,* and *c* transcripts localized to the PP (Fig. 2c, Supplementary Fig. 5) similar to *AtSWEET11*, *12,*

197   and *13* (Kim et al., 2020; Chen et al., 2012). Using three independent sets of probes, transcripts of

198   all three SWEET13s were almost exclusively found in the [ab]BS of rank-2 intermediate veins, which

9

199   are a special adaptation of C4 monocots (Langdale et al., 1988a) and serve as the main sites of

200   phloem loading (Fritz et al., 1989, 1983). *SWEET13a* was detected in both [ab]BS and PP in about

201   23% of the rank-2 intermediate veins. Thus, in the veins that are the main loading sites, sucrose

202   efflux towards the SE/CC for phloem loading must occur predominantly from the [ab]BS into the

203   apoplasm towards the phloem, and only to a smaller extent by direct release at the SE/CC from PP.

204   Rank-1 intermediate veins seemed to have a more balanced distribution of *SWEET13a* between

205   [ab]BS and PP. In major veins, SWEET13 transcripts were also present in the medial vascular

206   parenchyma, and the main path appeared to be through release from PP.

207   Since protein abundance does not always correlate with mRNA levels (Walley et al., 2016), we

208   evaluated the cell specificity of the SWEET13a protein. Maize lines were generated that stably

209   expressed translational GUS reporter fusions (*SWEET13a-GUS*) comprising 6 kb upstream of the

210   ATG and all exons and introns. Six transgenic lines from three independent transformation events

211   showed consistent localization of the SWEET13a-GUS fusion protein in the [ab]BS and phloem

212   parenchyma of rank-1 and -2 intermediate veins, and in the PP of the major veins (Fig. 4;

213   Supplementary Fig. 5). In summary, *in situ* hybridization and immunolocalization showed that

214   *SWEET13a, b, and c* transcripts and SWEET13a protein were not only found in the PP of maize,

215   but also in a subset of BSCs, specifically the [ab]BS. This is different from the cellular expression of

216   their orthologs in the dicot Arabidopsis, suggesting that an additional sucrose phloem loading

217   pathway evolved in C4 monocots (Langdale et al., 1988a).

218   ***SWEET13a- c* and *SUT1* sucrose transporters are expressed in complementary cell types**

219   Sucrose released from cells by SWEETs is taken up actively into the SE/CC by SUT1 H^{+}/sucrose

220   symporters (Riesmeier et al., 1994; Bürkle et al., 1998; Gottwald et al., 2000; Slewinski et al.,

221   2009). To directly compare SWEET13 and SUT localization, *in situ* hybridization was performed

222   in parallel using the same method from leaves at the same stages of development. *SUT1* RNA was

223   typically found in one or two cells in the phloem, which most likely represent companion cells,

10

224   where it is responsible for phloem loading. In rank-1 and major veins, *SUT1* mRNA was also

225   detected in the medial vascular parenchyma, where it likely contributes to sucrose retrieval (Heyser

226   et al., 1977). In our experiments, *SUT1* transcripts were not detected in bundle sheath cells,

227   consistent with *SUT1* expression below the detection limit in of our BSC single cell dataset (Fig.

228   2g-h; Supplementary Fig. 5).

229   **Abaxial BS transcripts are co-regulated during the sink-source transition**

230   In Arabidopsis, many PP-specific genes were found to also be co-regulated (Kim et al., 2020). We

231   therefore tested whether several of the transporter genes identified in [ab]BS might also be co-

232   regulated. *SUT1* H$^+$/sucrose symporter genes are typically lowly expressed in young net-importing

233   leaves and induced during the sink to source transition (Bürkle et al., 1998; Riesmeier et al., 1993).

234   RNA was extracted from different segments of leaf 3 of V2 plants, in which the tip had transitioned

235   to source while the base was still in the sink state (Tausta et al., 2014) (Fig. 5a) for qRT-PCR.

236   *SWEET13a,* and *UmamiT21, AAP45*, and *SUT1* had transcript levels that were 115-, 34-, 23-, and

237   10-fold higher, respectively, than in the tip of leaf 3 (source) compared to the base (sink) (Fig. 5a,

238   b). SWEET13a protein levels were also higher in source regions of the leaf (Fig. 5c). SWEET13a

239   was not detected in stem sections near the base of the plant, which contain whorls of developing

240   leaves, nor in root tip (Fig. 5d-f). In leaves, SWEET13a protein was not detectable in tissue other

241   than the tip of leaf 3, consistent with its role in phloem loading in source leaves The co-regulation

242   of [ab]BS-enriched genes during the developmental transition of leaves not only links them to transfer

243   of nutrients to the phloem, but also indicates that they are all controlled by the same regulatory

244   system.

245

11

DISCUSSION

While single cell sequencing was successfully used to identify the transcriptomes of vascular cells in Arabidopsis (Kim et al., 2020), the suberin-lignin barrier surrounding the bundle sheath of maize leaves prevented access to vascular cell transcriptomes in maize. With an optimized protocol, BSC were released and could be identified based on a broad range of known marker genes. BSC separated into two subclusters. mRNA for BSC markers such as *RBCS* and GS1-4 were present at equal levels in both subclusters, whereas others were specifically enriched in one of the two subclusters. Because only moderately and highly expressed mRNAs are captured with droplet-based scRNA-seq protocols such as 10x Chromium, we cannot exclude that transcripts that appear to be specific are present at lower levels in the other cell types. A major surprise was the finding that mRNA for all three *SWEET13* paralogs was present in BSCs, in clear contrast to the distribution of their orthologs in Arabidopsis (Chen et al., 2012). Since barley BSCs seem clearly differentiated, with S-type cells suspected to represent a preferential site of sucrose transfer into the phloem (Williams et al., 1989), we tested whether *SWEET13a*, *b*, and *c* mRNA would be present in adaxial and lateral BSCs. To our surprise, *in situ* hybridization and the analysis of translational GUS fusions showed that all three SWEET13s were preferentially expressed in the [ab]BS cells of rank-2 intermediate veins, which are considered the main sites of phloem loading in maize. In maize, these two abaxial BSCs are smaller compared to the medial BSCs (Bosabalidis et al., 1994). In rank-2 intermediate veins of maize, it appears that the [ab]BS cells may have recruited sucrose-transporting *SWEETs* to export sucrose toward the abaxially localized phloem (Fig. 6). This presents a unique pathway, in which BSCs likely export photosynthetically derived sucrose to the apoplasm of the phloem on the abaxial side of the leaf. Rank-2 veins are thought to be an emergent phenomenon of C4 grasses (Sedelnikova et al., 2018). Rank-2 veins increase the ratio of BS to MS cells, the vein density, and the capacity for nutrient transport. They appear to be the main path for

270   sucrose phloem loading. It is thus conceivable that the unique phloem loading pathway coevolved

271   with the evolution of the rank-2 intermediate veins.

272   Given the findings of Williams *et al* (Williams et al., 1989), which indicate that barley uses adaxial

273   and medial BSCs for phloem loading, our results suggest that the two species use distinct sets of

274   BSCs for transferring sucrose from the BS to the phloem. This may be generalizable to other C3

275   and C4 species, and it will be interesting to explore whether *SWEETs* are also present in medial

276   BSCs of barley. [ab]BS and [ad]BS transcript profiles are highly similar, possibly explaining why this

277   differentiation of BSCs had previously not been identified.

278   In rank-1 intermediate and major veins, *SWEET13a, b* and *c* transcripts were also detected in cells

279   in the vasculature that most likely correspond to phloem parenchyma, thus similar to the canonical

280   pathway in Arabidopsis (Chen et al., 2012; Cayla et al., 2019). Phylogenetic and functional analyses

281   had shown that the PP transporters AtSWEET11 and 12 from Arabidopsis are orthologous to the

282   three SWEET13 isoforms (Bezrutczyk et al., 2018). Subsequent to SWEET-mediated efflux,

283   sucrose is taken up actively by SUT1/SUC2 H^+/sucrose symporters in both maize and Arabidopsis

284   (Gottwald et al., 2000; Slewinski et al., 2009). This is supported by *in situ* hybridization of *SUT1*

285   in maize leaves (Supplementary Fig. 5). PP localization of *SUT1* is consistent with previously

286   published results (Baker et al., 2016). We could not confirm previous data that indicated that SUT1

287   may also be expressed substantially in BSCs (Supplementary Fig. 5). Localization of *SUT1* in

288   vascular parenchyma (VP) is consistent with a role in sucrose retrieval on the side of the phloem

289   that faces the xylem. Our data are compatible with the presence of two distinct sites for phloem

290   efflux in maize leaves, one from [ab]BS and a more standard path from PP (Fig. 6). This unique

291   pathway may be a specific adaptation of maize leaves in the context of C4 photosynthesis, to

292   provide higher rates of sucrose flux towards the phloem. No doubt, *SWEET13a, b* and *c* are key

293   players for phloem loading, though at present we cannot assess the relative contribution of this new

294   efflux step. This model could be tested by inhibiting SWEET activity specifically either in BSC or

13

295   PP. However, since transcription factors driving expression of genes specifically in maize [ab]BS or

296   PP are not currently known, this hypothesis could be tested by generation of lines in which

297   *SWEET13* mRNA levels have been repressed through BSC-specific RNAi.

298   Notably, transcripts for other transporter genes were also enriched in [ab]BS. This includes

299   UmamiT21a, a member of the UmamiT amino acid transporter family. One of the key findings

300   from the analysis of PP in Arabidopsis by scRNA-seq was that multiple members of this family

301   were specifically expressed in PP (Fig. 3, Table 1)(Kim et al., 2020). Since they appear to play

302   roles analogous to that of SWEETs in cellular efflux of amino acids in Arabidopsis, it appears that

303   [ab]BS, besides having clear BSC identity, has acquired components or subnetworks of the PP

304   identity. The co-regulation of at least some of the [ab]BS-enriched genes further strengthens this

305   hypothesis. Interestingly, we also observed a weak enrichment of the abaxial KANADI

306   transcription factor (Fig. 2a). KANADI plays a key role in determining abaxial identity in leaves

307   (Candela et al., 2008). We therefore hypothesize that one or several transcriptional regulators that

308   are involved in the regulation of the efflux of sucrose and amino acids from PP have been brought

309   under control of both a polarity cue and the BS identity cues in order to increase nutrient flux

310   towards the maize phloem. It will be fascinating to identify the transcription factors that are

311   involved in controlling the PP and BSC identities and to dissect the SWEET promoters to determine

312   which *cis*-elements are involved in the acquisition of the [ab]BS cell fate. Several transcriptional

313   regulators have been identified as candidates for the induction of [ab]BS cell fate; however, the

314   limitations of sequencing depth in 10x Genomics Chromium droplet-based scRNA-seq preclude a

315   comprehensive profiling of all transcriptional regulators. Methods that provide higher sensitivity

316   may help to address this aspect. Importantly, the [ab]BS genes identified provide unique insight into

317   the specialized nature of this cell type.

318   Comparison of this phenomenon in other grasses, those that use both C3 and C4 photosynthesis, as

319   well as a careful analysis of the evolution of rank-2 intermediate veins may provide insights into

14

320 how widely distributed this mechanism is and may provide hints regarding the evolution of this

321 regulatory rearrangement. Finally, new methods will be required to gain access to the vascular cells

322 of maize, which are not accessible through the current methods. In summary, scRNA-seq enabled

323 the identification of cells with a unique combination of properties on the adaxial side of the bundle

324 sheath, cells that play key roles in C4 photosynthesis. The identification of this new property may

325 be relevant to bioengineering of staple crops, for example, C4 rice.

326

327 **Materials Availability**

328 Plasmids generated in this study have been deposited to Addgene under the code Plasmid #159535.

329

330 **Data and Code Availability**

331 The raw data that support the findings of this study are available from the corresponding author

332 upon reasonable request. All sequencing data will be deposited in the Gene Expression Omnibus

333 GEO (www.ncbi.nlm.nih.gov/geo/) and the accession number will be updated here.

334

335 **METHOD DETAILS**

336 **Plant growth.**

337 *Zea mays* L. B73 seeds were germinated on filter paper with deionized, distilled water in darkness

338 at 22-25 °C and transferred to soil upon coleoptile emergence. Plants were subsequently grown at

339 28-30 °C in a greenhouse supplemented by sodium lamps (400 μmol m^{-2} s^{-1}) from 8:00-20:00.

340 Protoplasts for scRNA-seq were generated from the last 6 cm of the distal portion of V2 leaf 2. For

341 each pool of protoplasts tested, leaf segments from six concurrently grown plants were used. *In situ*

342 hybridization was performed on sections taken from the distal portion of leaf 2 of V2 plants, distal

343 portion of leaf 5 of V4 plants, and distal portion of the flag leaf from VT plants, with similar results.

344 All images shown are from V4 leaf 5. For GUS staining, tissue segments were taken 10 cm from

15

345   the tip of the third leaf below the flag leaf of T0 plants at growth stage VT (mature leaf tip), 4 cm

346   from the tip of leaf 3 of T1 V2 plants (seedling leaf tip), 12 cm from the tip of T1 V2 plants (seedling

347   leaf base), a stem section 1 cm above soil surface of T1 V2 plant (seedling stem), or the seminal

348   root tip from T1 V2 plant (seedling root).

349   **Genes analyzed here.**

350   Gene IDs are provided as Supplementary Table 4.

351   **Probe preparation for *in situ* hybridization.**

352   RNA was extracted from leaves of V2 B73 seedlings by phenol-chloroform extraction as previously

353   described (Bezrutczyk et al., 2018). cDNA synthesis was performed using QuantiTect Reverse

354   Transcription Kit (Qiagen, Hilden, Germany). cDNA was amplified for each gene (Supplementary

355   Table 5) using Takara PrimeSTAR GXL polymerase then subcloned into pJET1.2 using CloneJet

356   PCR cloning kit (ThermoFisher, Meerbusch, Germany). For *SWEET13a, b,* and *c*, three unique

357   regions in the 5'- and 3'-UTRs and in the coding region with lengths of ~100 bp were selected as

358   probe templates. The three probes specific for one of the genes were combined for detection of the

359   respective target gene. For *SUT1*, two regions in the 5'- and 3'-UTRs, unique to *SUT1* but common

360   to all six isoforms, were selected as probe templates. All cDNA sequence alignments were

361   performed using Geneious R11 (https://www.geneious.com) (Supplementary Fig. 6). Probe

362   template regions were amplified with SP6 sequences flanking the forward primers for the sense

363   probe, and reverse primers for antisense probes (Supplementary Table 5). The MEGAscript SP6

364   Transcription kit (ThermoFisher) was used with a 1:2 ratio of DIG-labelled UTP:UTP to generate

365   DIG-labelled probes. Probes were precipitated after DNAse reaction by addition of 2 mg/mL

366   glycogen, 0.1 volume 10% acetic acid, 0.1 volume NaOAc, and 2.5 volumes ethanol and

367   centrifuged at 4 °C at 20,000 x *g* for 30 min. Pellets were washed with 70% ethanol in DEPC-

368   treated water, allowed to dry, and resuspended in 25 µL RNAse-free 10 mM Tris-EDTA pH 8 and

369   25 µL formamide.

370   ***In situ* hybridization.**

371   *In situ* hybridization was adapted from Jackson and Simon lab protocols (Jackson, 1992; Stahl and

372   Simon, 2010). Leaf tip sections 1 cm in length were dissected from V2 or V5 plants into 4%

373   paraformaldehyde, vacuum-infiltrated for 10 min and fixed overnight at 4 °C. Dehydration by

374   ethanol series and paraplast embedding were performed as described (Malcomber and Kellogg,

375   2004). Sections (10 µm) were cut with a Leica RM 2155 microtome and mounted on ProbeOn Plus

376   slides (Fisher). After deparaffinization with Histoclear and rehydration by a decreasing ethanol

377   series, tissue was permeabilized in a 2 µg/mL proteinase K solution, washed with 0.2% glycine and

378   1x PBS (1.3 M NaCl, 0.07 M Na_2HPO_4, 0.03 M NaH_2PO_4) for 2 min, and re-fixed with 4%

379   paraformaldehyde for 10 min. Slides were washed with PBS and acetylated with 0.1 M

380   triethanolamine and acetic anhydride for 10 min, then washed and dehydrated with an increasing

381   ethanol series. Probes for each construct were mixed (e.g. all three antisense probes for

382   *SWEET13a*), diluted 1:50 with formamide, denatured at 95 °C for 3 min, and further diluted 1:4

383   with hybridization buffer (300 mM NaCl, 10mM NaH_2PO_4, 10mM Na_2HPO_4, 10mM Tris-Cl pH

384   6.8, 5 mM EDTA, 50% formamide, 12.5% dextran sulfate, 1.25mg/mL tRNA). Probe incubation

385   in slide pairs was performed at 55 °C overnight. Slides were rinsed three times with 0.2x SSC pH

386   7 (600 mM NaCl, 60 mM sodium citrate) at 55 °C for one hour, and washed with block reagent

387   solution (Roche), washed with BSA blocking solution (10 mg/mL BSA, 0.1 M Tris-Cl, 150 mL

388   NaCl, 0.3% Triton X-100) for 45 min, and incubated with anti-DIG antibody (Roche) for 2 hours

389   at 22 °C. Slides were rinsed four times with BSA block solution for 15 min each, in Buffer C (100

390   mM Tris pH 9.5, 50 mM $MgCl_2$, 100 mM NaCl) for 15 minutes, and incubated with 50 µL NBT

391   and 37.5 µL BCIP in 5 mL buffer C for 24-48 hours. Slides were washed with water, dehydrated

392   with an increasing ethanol series, and mounted with Eukitt Quick-hardening mounting medium.

393   Images were taken with an Olympus CKX53 cell culture microscope with EP50 camera. *In situ*

17

394   hybridization experiments for each gene (probe combination) were performed as (at minimum)

395   three independent experiments.

396   **Generation of ZmSWEET13-GUS constructs.**

397   *ZmSWEET13a* (Supplementary Table 4), including 5751 bp upstream of the start codon and 684

398   bp downstream of the stop codon, was isolated from B73 gDNA (Supplementary Table 5) and

399   inserted into pJET using the CloneJET PCR cloning kit. The final construct consists of GUSplus

400   inserted directly upstream of the *ZmSWEET13a* stop codon, preceded by a 9-alanine linker, in the

401   Golden Gate vector pGGBb-AG, the *in silico* cloning of which was performed using Geneious R11

402   (Supplementary Fig. 6). The assembly of all fragments with the vector pGGBb-AG was performed

403   using the Takara InFusion HD cloning kit, and validated by Sanger sequencing.

404

405   **Maize transformation.**

406   *Agrobacterium tumefaciens* strain EHA105 was transformed with the ZmSWEET13a:GUS vector

407   at the Crop Genome Engineering Facility at VIB Ghent (https://www.psb.ugent.be/cgef).

408   Transformed EHA105 carrying the respective plasmids was used to transform the inbred maize line

409   B104 via Agrobacterium-mediated transformation of 600 immature embryos according to

410   previously described methods (Coussens et al., 2012). In brief, callus formation was induced using

411   auxins and transgenic cells selected over several weeks using phosphinotricin (PPT) selection.

412   Plantlets were then regenerated on hormone-free medium, and presence of the transgene confirmed

413   using TraitCheck (Romer Labs; Butzbach, Germany) and PCR analysis. Three independent

414   transformation events were derived from different starting immature embryos, yielding six plants

415   in total: three plants from event A (pSWEET13a:SWEET13a:GUSplus[a]), two from event B

416   (pSWEET13a:SWEET13a:GUSplus[b]), and one from event C

417   (pSWEET13a:SWEET13a:GUSplus[c]).

GUS histochemistry.

Tissue segments were taken 10 cm from the tip of the third leaf below the flag leaf of T0 plants at growth stage VT (mature leaf tip), 4 cm from the tip of leaf 3 of T1 V2 plants (seedling leaf tip), 12 cm from the tip of T1 V2 plants (seedling leaf base), on the stem 1 cm above the soil surface of T1 V2 plant (seedling stem), or from the seminal root tip of T1 V2 plant (seedling root) at 13:00 o'clock. Tissue segments were dissected into cold acetone and vacuum-infiltrated for two min, vacuum infiltrated with GUS wash buffer (20 mM EDTA, 40 mM $C_6N_6FeK_3$, 40 mM $C_6FeK_4N_6$, 20% methanol, 57.6 mM Na_2HPO_4, 42 mM NaH_2PO_4, 0.1% Triton X-100), and incubated with GUS wash buffer including 0.2% X-Gluc at 37°C for 1-48 hours. Sections were dehydrated in 20%, 30%, 50% ethanol for 30 min, fixed in FAA (50% ethanol, 3.7% formaldehyde, 5% acetic acid) for 30 min, and further dehydrated in 75% and 100% ethanol. Embedding was performed by incubating sections at 60 °C in tert-butyl ethanol:paraplast dilutions at 3:1, 1:1, and 1:3 ratios. Melted paraplast (100%) was changed twice daily for three days. Paraplast-embedded tissue was poured into blocks, and 10-μm sections were cut with a Leica RM 2155 microtome. Sections were mounted on SUPERFROST PLUS Gold Slides (Thermo Scientific), deparaffinized with Histoclear, and mounted with Eukitt Quick-hardening mounting medium.

Single cell sequencing: protoplast preparation.

Tissue was sampled from the distal portion of leaf 2 (from 1 cm to 7 cm, as measured from the tip) from V2 plants. This region was selected because it is thought to be non-expanding, non-differentiating source tissue based on results from the RNAseq-defined developmental transcriptome of the maize leaf (Li et al., 2010). Leaf segments were harvested at 9:00 am, and tape was applied to adaxial epidermis to stabilize the tissue, which was scored every 5 mm from the midvein to leaf edge with a razor manifold consisting of scalpel blades taped together to ensure minimum distance between scores. Tape sections were placed abaxial-side down in pretreatment solution (2 mM L-cysteine, 164 mM sorbitol) and vacuum-infiltrated for 10 min with 2 min of

19

443 active pumping. Tape sections were incubated with gentle agitation (30 rpm, IKA Rocker 3D

444 orbital shaker) for an additional 20 min in pre-treatment solution, then transferred to enzyme

445 solution (cellulase "Onozuka" RS 1.25%, cellulase "Onozuka" R-10 1.25%, pectolyase Y-23 0.4%,

446 macerozyme R-10 0.42%, sorbitol 0.4 M, MES 20 mM, KCL 20 mM, $CaCl_2$ 10 mM, BSA 0.1%,

447 ß-mercaptoethanol 0.06%) for 3.5 h with gentle agitation (30 rpm on orbital shaker). Protoplasts

448 were filtered through a Corning 70-µm nylon mesh strainer and centrifuged in a round bottom tube

449 for 1.5 min at 100 x g. Enzyme solution was gently removed and replaced with cold wash solution

450 (sorbitol 0.4M, MES 20mM, KCl 20mM, $CaCl_2$ 10mM, BSA 0.1%). Protoplasts were carefully

451 resuspended in wash solution and centrifuged for 30 seconds at 100 x g, then strained through a

452 70-µm Scienceware Flowmi Cell Strainer to remove large debris. Washing solution steps were

453 repeated four additional times to remove chloroplasts and small debris. Cell viability and

454 concentration were quantified under an Olympus CKX53 cell culture microscope: 1 µL 0.4%

455 Trypan blue was added to 9 µL of resuspended protoplasts in wash solution and pipetted into the

456 chamber of a C-Chip Neubauer Improved Disposable Haemocytometer (NanoEntek; Seoul, South

457 Korea); healthy (unstained) cells were counted. Protoplasts were resuspended to a concentration of

458 1,200 cells /µL. A variety of approaches to degrade the suberin-lignin-containing bundle sheath

459 cell walls with the addition of other enzymes failed to produce healthy cells: Laccase (Sigma) and

460 manganese peroxidase (Sigma), as well as enzymes provided by Novozymes (Copenhagen,

461 Denmark), namely a cutinase, a fungal carbohydrase blend produced in *Aspergillus aculeatus*, a

462 fungal beta-glucanase blend produced in *Humicola insolens*, a pectinase preparation produced in

463 *Aspergillus*, a xylanase blend, and a multi-enzyme complex containing carbohydrases, including

464 arabanase, cellulase, beta-glucanase, hemicellulose and xylanase, were each added to the existing

465 protocol to a final concentration of 1-2% active enzyme weight/vol. Visual inspection of protoplasts

466 during isolation revealed that addition of these enzymes caused protoplasts to rupture.

467 **Protoplast protocol optimization**

20

468 Several variations of the above protocol were tested prior to the final protoplast preparation, and

469 the presence of diverse cell types was verified by qRT-PCR using primers specific to *MDH6*, *ME1*,

470 *SWEET13a*, *SWEET13b*, and *SWEET13c* (Supplementary Table 5). Briefly, RNA was extracted

471 from protoplasts using the RNEasy Mini Kit, and first strand cDNA was synthesized using

472 Quantitect reverse transcription kit (Qiagen, Hilden, Germany). Quantitative reverse transcription

473 PCR (qRT-PCR) was performed using Roche LightCycler 480 SYBR Green I Master polymerase

474 on a Stratagene Mx3000P, and relative expression of transporter genes was calculated relative to

475 18S and Actin using the $2^{-\Delta CT}$ method. Modifications to the standard protoplast isolation protocol

476 of 2 h in enzyme solution (see previous section) (Protocol 1) included doubling the concentration

477 of enzymes in solution (Protocol 2), isolating BS strands released after 2 h followed by continued

478 incubation of filtered BS strands in fresh enzyme solution to deplete mesophyll cells (Protocol 3),

479 and incubating the leaf tissue in pretreatment solution (Protocol 4) (2 mM L-cysteine and164 mM

480 sorbitol). The protocol which yielded the highest ratio of BS:MS marker genes (*ME1*: *MDH6*)

481 included a pretreatment incubation step and 1x enzyme solution (Supplementary Fig. 1).

482 **Cell partitioning, library prep, and sequencing.**

483 To aim for partitioning of 7,000 cells, with the expectation that 3,500 cells would be sequenced, 6

484 µL of the protoplast suspension with an estimated 1,200 cells/µL was applied to the 10x Genomics

485 Chromium microfluidic chip (Chemistry V3.0). Thereafter the standard manufacturer's protocol

486 was followed. Twelve cycles were used for cDNA amplification, and the completed cDNA library

487 was quantified using an Agilent AATI Fragment Analyzer. Sequencing was performed at

488 Novogene (Sacramento, CA, USA) on a single lane with the Hi-Seq platform and the standard

489 PE150 sequencing parameters.

490 **Generation of single-cell expression matrices**

491 Cellranger count (10x Genomics) was used to process fastq files provided by Novogene, with

492 read 1 trimmed to 26 bp (r1-length=26), as the first 26 bp of a 10x library R1 comprise the cell

21

493   barcode and UMI index, and the remaining comprises poly-A tail with no further information. A

494   formatted reference genome was generated using Cellranger mkref using the maize B73 RefGen

495   4 (Jiao et al., 2017) whole genome sequence and annotation (fasta and gff3 downloaded from

496   Ensembl B73 RefGen V4), to which reads were aligned using STAR (Dobin et al., 2013). For

497   analysis of single cell sequencing data, see "Quantification and Statistical Analysis" section

498   below.

499   **Phylogeny of UmamiT transporters**

500   BLAST results from the seed sequence AtUmamiT12 (At2g37460) to maize (AGP v4 (Jiao et al.,

501   2017) and barley (IBSC v2 (Mascher et al., 2017)) were combined with BioMart (Smedley et al.,

502   2009) results and filtered for the WAT1-related protein domain (panther ID PTHR31218). Genes

503   passing this filter were selected as UmamiT family candidate genes. Two trees were generated: one

504   using an alignment of all known splice variants, and one with only the representative transcript,

505   with similar results. Alignment was performed in MEGA7 (Kumar et al., 2016) using MUSCLE

506   with the following parameters: gap open penalty -2.9, gap extend penalty 0, hydrophobicity

507   multiplier 1.2, max iterations 8, clustering method UPGMA for iteration 1, 2; UPGMB for all

508   subsequent iterations, and lambda 24. The maximum likelihood tree was created from these

509   alignments using IQTREE webserver (Trifinopoulos et al., 2016) using the BLOSUM62

510   substitution model and 1000 bootstraps.

511

512   **QUANTIFICATION AND STATISTICAL ANALYSIS**

513

514   **Sample selection for scRNA-Seq, qRT-PCR, and RNAseq**

515   Plants chosen for protoplast release, qPCR, and RNAseq were randomly selected from among a

516   larger number of individuals which had been grown concurrently and were at the same growth

517   stage. True biological replicates (i.e., independently grown plants) were used as replicates for

518   statistical analyses. The number of plants per sample and number of replicates is given in the Figure

519   legends or in specific methods sections. To ensure reproducibility, the plants used in successive

520   experiments were grown in the same greenhouse under controlled conditions. Samples for a given

521   experiment were taken at the same developmental stage, at the same time of day.

522

523   **Dimensionality reduction and cell clustering**

524   The Seurat R package (v3.1)(Butler et al., 2018) was used for dimensionality reduction analysis

525   and dataset filtering. To remove cells with low mRNA count (nFeature_RNA) and doublets, as well

526   as damaged cells with high chloroplast (pt) or mitochondria (mt) genome-derived transcripts, cells

527   were filtered (percent.pt <4 & percent.mt <0.75 & nFeature_RNA >1800 & nFeature_RNA

528   <7000). Normalization, scaling, and variable feature detection were performed using SCTransform

529   (Hafemeister and Satija, 2019). Cells were clustered using FindNeighbors to create a K-nearest

530   neighbors graph using the first 50 principle components. FindClusters was used to iteratively group

531   cells using a resolution of 0.2 or 23. These clusters were used as input for non-linear dimensional

532   reduction using Uniform Manifold Approximation and Projection (UMAP)(McInnes et al., 2018).

533   **Differential gene expression analysis across clusters**

534   Genes differentially expressed across clusters or subclusters were identified by comparing average

535   normalized mRNA counts in cells of a given cluster to that of cells in all other clusters using the

536   Seurat function FindMarkers. Genes with an FDR corrected P-value <0.05 and an average logFC

537   >0.5 were considered marker genes.

538   **Identification of cluster identities**

539   Canonical C4 photosynthesis-related genes were used as markers to define MSC and BSC clusters

540   (Denton et al., 2017) (Supplementary Table 1). The cluster identified as BSC was subdivided into

541   two subclusters when FindClusters was applied with a resolution of 23, and differential gene

542   expression analysis was performed on these two subclusters with FindMarkers (for subclusters:

543   logFC >0.5, FDR ≤0.01).

544   qRT-PCR of transporter genes in seedling leaf

545   Leaf segments were harvested from the distal and proximal end (tip and base) of leaf 3 of early V2

546   plants at 13:00. Tissue was ground in liquid nitrogen and RNA extracted as previously described

547   (Bezrutczyk et al., 2018). First strand cDNA was synthesized using Quantitect reverse transcription

548   kit (Qiagen). qRT-PCR to determine relative mRNA levels was performed using a Stratagene

549   Mx3000P with primers for *18S, Actin, SWEET13a, 13b, 13c, SUT1, UmamiT21a*, and *STP3*

550   (Supplementary Table 5). Relative expression of transporter genes was calculated relative to *18S*

551   and *Actin* using the $2^{-\Delta CT}$ method for quantification, with similar results. Values shown in Figure

552   5b are the average of three technical (qRT-PCR) replicates of three pools of two plants; error bars

553   represent SEM. Students two-tailed paired t-test values are shown. Two independent repeats

554   confirmed the data.

555   Gene Ontology term analysis for mesophyll clusters

556   Marker genes for each of the five mesophyll clusters (LogFC >0.5; FDR-adjusted p-value <0.05)

557   were used as input for Gene Ontology (Ashburner et al., 2000; The Gene Ontology Consortium,

558   2018) analysis via the online portal GO Gene Ontology database (doi: 10.5281/zenodo.3727280;

559   released 2020-03-23). GO terms with FDR-corrected p-values <0.05 can be found in

560   Supplementary Table 3.

561   Protoplast and bulk leaf tissue RNAseq

562   Protoplasts were generated according to the previously described method. Whole leaf tissue from

563   sibling plants was ground in liquid nitrogen at the time leaf tissue was harvested for protoplast

564   isolation. RNA from two pools of protoplasts made from four leaves each (P1 and P2), and two

565   pools of four whole leaf segments each (L1 and L2) was extracted using the RNEasy Mini Kit

566   (Qiagen), and four cDNA libraries were generated using the NEBNext Ultra DNA Library Prep Kit

567   for Illumina (New England Biolabs, MA, USA) with modifications to select for 250-500 bp

568   fragments. Sequencing of the four libraries was performed at Novogene (Sacramento, CA, USA)

569   on a single lane with the Hi-Seq platform and the standard PE150 sequencing parameters. Reads

570   were analyzed using a custom implementation of the Wyseq RNAseq analysis pipeline

571   (https://github.com/astauff/WySeq). Briefly, reads were trimmed using TrimGalore (v 0.6.5) and

572   aligned to the AGPv4 B73 reference genome using STAR (v 2.5.1b). Counts were generated using

573   Subread featureCounts (v 2.0.1), and differential expression was analyzed using the R-packages

574   EdgeR (v3.30.3) and limma (v 3.44.3) using trimmed mean M-value (TMM) normalization factors.

575   Reads corresponding to BSC-specific genes and MS-specific genes were normalized separately to

576   compensate for the expected difference in cell populations represented in protoplasts and whole

577   leaf tissue. Genes were filtered to remove those with a coefficient of variation >75th percentile

578   within replicate groups prior to correlation analysis. Pearson correlation (Supplementary Fig. 7)

579   and differentially expressed genes specific to BS and MS-cells (logFC > 1 or < -1) are presented

580   (Supplementary Table 6). None of the genes in the [ab]BS subclusters were induced by protoplast

581   isolation. Rather, several showed reduced mRNA levels in the protoplast sample.

582

583

REFERENCES

Ashburner, M. et al. (2000). Gene ontology: tool for the unification of biology. The Gene Ontology Consortium. Nat. Genet. **25**: 25–29.

Baker, R.F., Leach, K.A., Boyer, N.R., Swyers, M.J., Benitez-Alfonso, Y., Skopelitis, T., Luo, A., Sylvester, A., Jackson, D., and Braun, D.M. (2016). Sucrose transporter ZmSut1 expression and localization uncover new insights into sucrose phloem loading. Plant Physiol. **172**: 1876–1898.

Bezrutczyk, M., Hartwig, T., Horschman, M., Char, S.N., Yang, J., Yang, B., Frommer, W.B., and Sosso, D. (2018). Impaired phloem loading in *zmsweet13a,b,c* sucrose transporter triple knock-out mutants in *Zea mays*. New Phytol. **218**: 594–603.

Bosabalidis, A.M., Evert, R.F., and Russin, W.A. (1994). Ontogeny of the vascular bundles and contiguous tissues in the maize leaf blade. Am. J. Bot. **81**: 745–752.

Bürkle, L., Hibberd, J.M., Quick, W.P., Kühn, C., Hirner, B., and Frommer, W.B. (1998). The H^+-sucrose cotransporter NtSUT1 is essential for sugar export from tobacco leaves. Plant Physiol. **118**: 59–68.

Butler, A., Hoffman, P., Smibert, P., Papalexi, E., and Satija, R. (2018). Integrating single-cell transcriptomic data across different conditions, technologies, and species. Nat. Biotechnol. **36**: 411–420.

Candela, H., Johnston, R., Gerhold, A., Foster, T., and Hake, S. (2008). The *milkweed pod1* gene encodes a KANADI protein that is required for abaxial/adaxial patterning in maize leaves. Plant Cell **20**: 2073.

Cayla, T., Le Hir, R., and Dinant, S. (2019). Live-cell imaging of fluorescently tagged phloem proteins with confocal microscopy. Methods Mol. Biol. Clifton NJ **2014**: 95–108.

Chang, Y.-M., Liu, W.-Y., Shih, A.C.-C., Shen, M.-N., Lu, C.-H., Lu, M.-Y.J., Yang, H.-W., Wang, T.-Y., Chen, S.C.-C., Chen, S.M., Li, W.-H., and Ku, M.S.B. (2012). Characterizing regulatory and functional differentiation between maize mesophyll and bundle sheath cells by transcriptomic analysis. Plant Physiol. **160**: 165.

Chastain, C.J., Baird, L.M., Walker, M.T., Bergman, C.C., Novbatova, G.T., Mamani-Quispe, C.S., and Burnell, J.N. (2017). Maize leaf PPDK regulatory protein isoform-2 is specific to bundle sheath chloroplasts and paradoxically lacks a Pi-dependent PPDK activation activity. J. Exp. Bot. **69**: 1171–1181.

Chen, L.Q., Qu, X.Q., Hou, B.H., Sosso, D., Osorio, S., Fernie, A.R., and Frommer, W.B. (2012). Sucrose efflux mediated by SWEET proteins as a key step for phloem transport. Science **335**: 207–11.

622 **Coussens, G., Aesaert, S., Verelst, W., Demeulenaere, M., De Buck, S., Njuguna, E.,**
623   **Inzé, D., and Van Lijsebettens, M.** (2012). *Brachypodium distachyon* promoters
624   as efficient building blocks for transgenic research in maize. J. Exp. Bot. **63**:
625   4263–4273.

626 **Deng, L.** (2014). A Genome-Wide Analysis of the AAAP Gene Family in Maize. J.
627   Proteomics Bioinform. **07**.

628 **Denton, A.K., Maß, J., Külahoglu, C., Lercher, M.J., Bräutigam, A., and Weber,**
629   **A.P.M.** (2017). Freeze-quenched maize mesophyll and bundle sheath separation
630   uncovers bias in previous tissue-specific RNA-Seq data. J. Exp. Bot. **68**: 147–160.

631 **Dobin, A., Davis, C.A., Schlesinger, F., Drenkow, J., Zaleski, C., Jha, S., Batut, P.,**
632   **Chaisson, M., and Gingeras, T.R.** (2013). STAR: ultrafast universal RNA-seq
633   aligner. Bioinformatics **29**: 15–21.

634 **Friso, G., Majeran, W., Huang, M., Sun, Q., and van Wijk, K.J.** (2010).
635   Reconstruction of metabolic pathways, protein expression, and homeostasis
636   machineries across maize bundle sheath and mesophyll chloroplasts: large-scale
637   quantitative proteomics using the first maize genome assembly. Plant Physiol.
638   **152**: 1219.

639 **Fritz, E., Evert, R.F., and Heyser, W.** (1983). Microautoradiographic studies of phloem
640   loading and transport in the leaf of *Zea mays* L. Planta **159**: 193–206.

641 **Fritz, E., Evert, R.F., and Nasse, H.** (1989). Loading and transport of assimilates in
642   different maize leaf bundles. Planta **178**: 1–9.

643 **The Gene Ontology Consortium** (2018). The Gene Ontology Resource: 20 years and
644   still GOing strong. Nucleic Acids Res. **47**: D330–D338.

645 **Gottwald, J.R., Krysan, P.J., Young, J.C., Evert, R.F., and Sussman, M.R.** (2000).
646   Genetic evidence for the *in planta* role of phloem-specific plasma membrane
647   sucrose transporters. Proc. Natl. Acad. Sci. **97**: 13979.

648 **Hafemeister, C. and Satija, R.** (2019). Normalization and variance stabilization of
649   single-cell RNA-seq data using regularized negative binomial regression. Genome
650   Biol. **20**: 296.

651 **Henderson, D.C., Zhang, X., Brooks III, L., and Scanlon, M.J.** (2006). RAGGED
652   SEEDLING2 is required for expression of KANADI2 and REVOLUTA
653   homologues in the maize shoot apex. genesis **44**: 372–382.

654 **Heyser, W., Heyser, R., Eschrich, W., and Fritz, E.** (1977). The influence of externally
655   supplied sucrose on phloem transport in the maize leaf strip. Planta **137**: 145–151.

656 **Jackson, D.** (1992). *In situ* hybridization in plants. In Molecular Plant Pathology. A
657   practical approach, S.J. Gurr, M.J. McPherson, and D.J. Bowles, eds (Oxford
658   University Press: Oxford), pp. 163–174.

659 **Jiao, Y. et al.** (2017). Improved maize reference genome with single-molecule
660   technologies. Nature **546**: 524–527.

661 **Juarez, M.T., Kui, J.S., Thomas, J., Heller, B.A., and Timmermans, M.C.P.** (2004a).
662   microRNA-mediated repression of rolled leaf1 specifies maize leaf polarity.
663   Nature **428**: 84–88.

664 **Juarez, M.T., Twigg, R.W., and Timmermans, M.C.P.** (2004b). Specification of
665   adaxial cell fate during maize leaf development. Development **131**: 4533.

666 **Kanai, R. and Edwards, G.E.** (1973). Separation of mesophyll protoplasts and bundle
667   sheath cells from maize leaves for photosynthetic studies. Plant Physiol. **51**:
668   1133–1137.

669 **Kim, J.Y., Symeonidi, E., Tin, P.Y., Denyer, T., Weidauer, D., Miras, M., Wudick,**
670   **M., Lercher, M., Timmermans, M.C.P., and Frommer, W.B.** (2020). Unique
671   properties of leaf phloem cells revealed by single cell transcriptomics. **submitted**.

672 **Kumar, S., Stecher, G., and Tamura, K.** (2016). MEGA7: Molecular Evolutionary
673   Genetics Analysis version 7.0 for bigger datasets. Mol. Biol. Evol. **33**: 1870–
674   1874.

675 **Langdale, J.A., Lane, B., Freeling, M., and Nelson, T.** (1989). Cell lineage analysis of
676   maize bundle sheath and mesophyll cells. Dev. Biol. **133**: 128–139.

677 **Langdale, J.A., Rothermel, B.A., and Nelson, T.** (1988a). Cellular pattern of
678   photosynthetic gene expression in developing maize leaves. Genes Dev. **2**: 106–
679   115.

680 **Langdale, J.A., Zelitch, I., Miller, E., and Nelson, T.** (1988b). Cell position and light
681   influence C4 versus C3 patterns of photosynthetic gene expression in maize.
682   EMBO J. **7**: 3643–3651.

683 **Li, P. et al.** (2010). The developmental dynamics of the maize leaf transcriptome. Nat
684   Genet **42**: 1060–7.

685 **Malcomber, S.T. and Kellogg, E.A.** (2004). Heterogeneous expression patterns and
686   separate roles of the *SEPALLATA* gene *LEAFY HULL STERILE1* in grasses. Plant
687   Cell **16**: 1692.

688 **Martin, A. et al.** (2006). Two cytosolic glutamine synthetase isoforms of maize are
689   specifically involved in the control of grain production. Plant Cell **18**: 3252–3274.

690 **Mascher, M. et al.** (2017). A chromosome conformation capture ordered sequence of the
691   barley genome. Nature **544**: 427–433.

692 **McInnes, L., Healy, J., and Melville, J.** (2018). UMAP: uniform manifold
693   approximation and projection for dimension reduction. arXiv **eprint**
694   **arXiv:1802.03426**.

695 **Ortiz-Ramírez, C., Arevalo, E.D., Xu, X., Jackson, D.P., and Birnbaum, K.D.** (2018).
696   An efficient cell sorting protocol for maize protoplasts. Curr. Protoc. Plant Biol.
697   **3**: e20072–e20072.

698 **Riesmeier, J.W., Hirner, B., and Frommer, W.B.** (1993). Potato sucrose transporter
699   expression in minor veins indicates a role in phloem loading. Plant Cell **5**: 1591–
700   1598.

701 **Riesmeier, J.W., Willmitzer, L., and Frommer, W.B.** (1994). Evidence for an essential
702   role of the sucrose transporter in phloem loading and assimilate partitioning.
703   EMBO J. **13**: 1–7.

704 **Sedelnikova, O.V., Hughes, T.E., and Langdale, J.A.** (2018). Understanding the
705   genetic basis of C4 Kranz anatomy with a view to engineering C3 crops. Annu.
706   Rev. Genet. **52**: 249–270.

707 **Slewinski, T.L., Meeley, R., and Braun, D.M.** (2009). Sucrose transporter1 functions in
708   phloem loading in maize leaves. J. Exp. Bot. **60**: 881–892.

709 **Smedley, D., Haider, S., Ballester, B., Holland, R., London, D., Thorisson, G., and**
710   **Kasprzyk, A.** (2009). BioMart – biological queries made easy. BMC Genomics
711   **10**: 22.

712 **Stahl, Y. and Simon, R.** (2010). mRNA detection by whole mount *in situ* hybridization
713   (WISH) or sectioned tissue *in situ* hybridization (SISH) in Arabidopsis. Methods
714   Mol. Biol. Clifton NJ **655**: 239–251.

715 **Tausta, S.L., Li, P., Si, Y., Gandotra, N., Liu, P., Sun, Q., Brutnell, T.P., and Nelson,**
716   **T.** (2014). Developmental dynamics of Kranz cell transcriptional specificity in
717   maize leaf reveals early onset of C4-related processes. J. Exp. Bot. **65**: 3543–
718   3555.

719 **Trifinopoulos, J., Nguyen, L.-T., von Haeseler, A., and Minh, B.Q.** (2016). W-IQ-
720   TREE: a fast online phylogenetic tool for maximum likelihood analysis. Nucleic
721   Acids Res. **44**: W232–W235.

722 **Walley, J.W., Sartor, R.C., Shen, Z., Schmitz, R.J., Wu, K.J., Urich, M.A., Nery,**
723   **J.R., Smith, L.G., Schnable, J.C., Ecker, J.R., and Briggs, S.P.** (2016).
724   Integration of omic networks in a developmental atlas of maize. Science **353**:
725   814–818.

726 **Williams, M.L., Farrar, J.F., and Pollock, C.J.** (1989). Cell specialization within the
727   parenchymatous bundle sheath of barley. Plant Cell Environ. **12**: 909–918.

728 **Wu, Y., Lee, S.-K., Yoo, Y., Wei, J., Kwon, S.-Y., Lee, S.-W., Jeon, J.-S., and An, G.**
729   (2018). Rice Transcription Factor OsDOF11 Modulates Sugar Transport by
730   Promoting Expression of Sucrose Transporter and SWEET Genes. Mol. Plant **11**:
731   833–845.

732

741

742   **AUTHOR CONTRIBUTIONS**

743   Conceptualization, M.B., J.K., W.B.F.; Methodology, M.B., C.P.S.K, T.H., T.L.;

744   Investigation, M.B, N.Z, T.L, C.P.S.K.; Resources, K.K, W.B.F.; Writing, M.B., W.B.F.;

745   Supervision, J.K., W.B.F.

746

747   **DECLARATION OF INTERESTS**

748   The authors do not declare any competing interests.

749 **MAIN FIGURES**

750 Table 1. Genes of interest differentially expressed between clusters adBS and abBS

751 Figure 1. Mesophyll and bundle sheath clusters show canonical expression of C4 photosynthesis

752 genes

753 Figure 2. Abaxial BS cluster is enriched for genes encoding transport proteins

754 Figure 3. Arabidopsis homologs of maize [ab]BS-specific genes are expressed in Arabidopsis phloem

755 parenchyma

756 Figure 4. SWEET13a protein is localized to abaxial BSC of rank-2 veins

757 Figure 5. Abaxial BS transcripts are co-regulated during the sink-source transition

758 Figure 6. Phloem loading occurs via the abBS in maize

759

760 **SUPPLEMENTARY DATA**

761 Supplementary. Fig. 1. qRT-PCR of putative BSC and vascular-expressed genes as an indication

762 of protoplast cell type diversity prior to sequencing

763 Supplementary. Fig. 2. Expression patterns of canonical C4 photosynthesis-related genes in single

764 cell sequencing dataset

765 Supplementary. Fig. 3. UMAP plots of glutamine synthetase, transport-related proteins, and

766 transcription factors in bundle sheath cells

767 Supplementary. Fig. 4. Neighbor joining tree of family of UmamiT amino acid transporters in

768 Arabidopsis, maize, and barley veins

769 Supplementary. Fig. 5. SWEET and SUT mRNA localization and SWEET13a protein localization

770 in rank-2 intermediate and major

771 Supplementary. Fig. 6. Probe design for in situ hybridization and pSWEET13a:SWEET13a:GUS

772 construct schematic

773 Supplementary. Fig. 7. Correlation of mRNA counts between protoplasted cells and whole leaf

774

775 Supplementary. Table 1. Marker genes for all clusters

776 Supplementary. Table 2. mRNA enrichment of C4 photosynthesis-related genes in MS and BS

777 clusters

778 Supplementary. Table 3. GO term analysis for MS clusters

779 Supplementary. Table 4. Genes used in this study

780 Supplementary. Table 5. Primers

781 Supplementary. Table 6. Protoplast enriched, depleted mRNAs

782 Supplementary. Text 1. A subset of mesophyll cells appears to be specialized in iron metabolism

Table 1.

^{ab}BS cluster	logFC	FDR	description
Zm00001d023677	4.990	2.3E-08	**SWEET13a**
Zm00001d041067	3.959	3.2E-08	**SWEET13c**
Zm00001d016625	3.675	3.3E-07	Os02g0519800 protein
Zm00001d023673	2.156	2.2E-06	**SWEET13b**
Zm00001d035717	2.140	3.3E-07	**UmamiT21a**
Zm00001d033551	1.412	3.3E-07	Phosphoglycerate mutase-like family protein
Zm00001d033980	1.252	4.5E-03	*Ustilago maydis* induced12
Zm00001d019062	1.180	2.9E-04	**Membrane H⁺ATPase3**
Zm00001d035243	1.123	1.4E-03	**AAP45**
Zm00001d038753	1.114	7.7E-05	Ubiquitin domain-containing protein
Zm00001d017966	1.098	5.0E-04	Dihydropyrimidine dehydrogenase (NADP(+)) chloroplastic
Zm00001d012231	1.055	9.2E-04	**AAP56**
Zm00001d018867	0.992	1.1E-05	Syntaxin 132
Zm00001d000299	0.920	1.1E-05	Endosomal targeting BRO1-like domain-containing protein
Zm00001d002489	0.809	4.5E-03	PLATZ transcription factor family protein
Zm00001d035651	0.806	5.0E-04	DNA binding with one finger3
Zm00001d027268	0.753	6.5E-04	**STP3 (sugar transport protein 3)**
Zm00001d005344	0.737	1.4E-03	Histidine-containing phosphotransfer protein 2
Zm00001d013296	0.737	4.5E-03	ATP sulfurylase 1
Zm00001d030103	0.735	8.1E-03	Probable xyloglucan endotransglucosylase/hydrolase protein
Zm00001d052038	0.723	3.8E-03	Putative HLH DNA-binding domain superfamily protein
Zm00001d012559	0.692	2.1E-03	Stomatal closure-related actin-binding protein 1
Zm00001d015025	0.684	4.5E-03	AMP binding protein
Zm00001d038768	0.636	5.0E-03	Reticulon-like protein B4
Zm00001d044768	0.633	3.8E-03	**Protein NRT1/ PTR FAMILY 5.8**
Zm00001d033981	0.633	4.8E-03	ATP sulfurylase 1
Zm00001d015618	0.619	8.1E-03	Probable cinnamyl alcohol dehydrogenase
Zm00001d041710	0.597	5.0E-03	Glutathione synthetase chloroplastic
Zm00001d036401	0.596	5.0E-03	Endoplasmin homolog
Zm00001d018758	0.584	8.1E-03	Succinate dehydrogenase1
Zm00001d019670	0.578	8.5E-03	Kinesin-like protein KIN-4A
Zm00001d022042	0.574	9.4E-04	Eukaryotic translation initiation factor 5A
Zm00001d049597	0.567	4.9E-03	External alternative NAD(P)H-ubiquinone oxidoreductase B4
Zm00001d016662	0.536	3.8E-03	
Zm00001d018178	0.535	4.7E-03	bZIP4 (ABSCISIC ACID-INSENSITIVE 5-like protein 5)
Zm00001d032249	0.532	2.1E-03	KANADI 1
Zm00001d002625	0.531	3.4E-03	Probable methyltransferase PMT15
Zm00001d021773	0.517	9.9E-03	
Zm00001d039270	0.512	3.5E-03	Glutaredoxin family protein

Table 1.

Genes of interest differentially expressed between clusters ^{ab}BS and ^{ad}BS. 9 out of 39 genes specific to the ^{ab}BS cluster are specific to transmembrane transport (bold). Criteria for inclusion were average log fold change > 0.5 for all cells in subcluster and FDR-adjusted p-value < .01. The ^{ab}BSC specificity was validated for three genes, *SWEET13a*, *b* and *c*. Whether genes with lower FDR-adjusted p-values also show high specificity will require experimental validation.
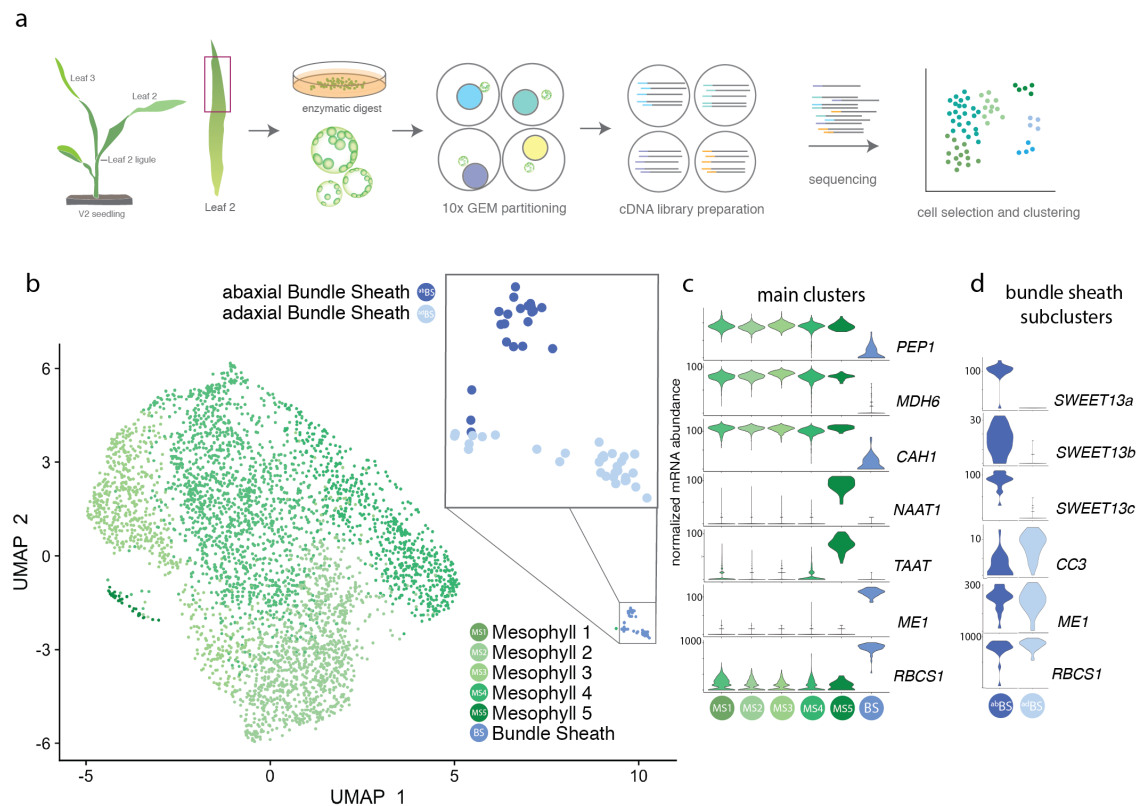
Figure 1.

Figure 1. Mesophyll and bundle sheath clusters show canonical expression of C4 photosynthesis genes a. Illustration of protoplasting, 10x Chromium Gel Bead-in-Emulsion (GEM) partitioning and cDNA synthesis, RNA sequencing, and data analysis. **b.** UMAP plot showing 2D representation of cell relationships in multidimensional space; bundle sheath cells separate into 2 subclusters at higher resolution (inset). The "upper" and "lower" cluster were later determined to correspond to abaxial and adaxial BSC (Fig. 2), and are therefore named [ab]BS and [ad]BS **c.** Violin plots showing distribution of normalized mRNA counts of marker genes for cells in each cluster. Genes were canonical C4 markers (*PEP1, MDH6, CA, ME1, RBCS*) or genes that identify unique clusters (*NAAT1, TAAT*). **d.** Violin plots showing normalized mRNA levels of genes differentially expressed between [ab]BS and BS[ad] subclusters (*SWEET13a, b, and c, CC3*) and of example genes highly expressed in both clusters (*ME1, RBCS1*). Gene IDs are provided in Supplementary Table 4.

Figure 2.
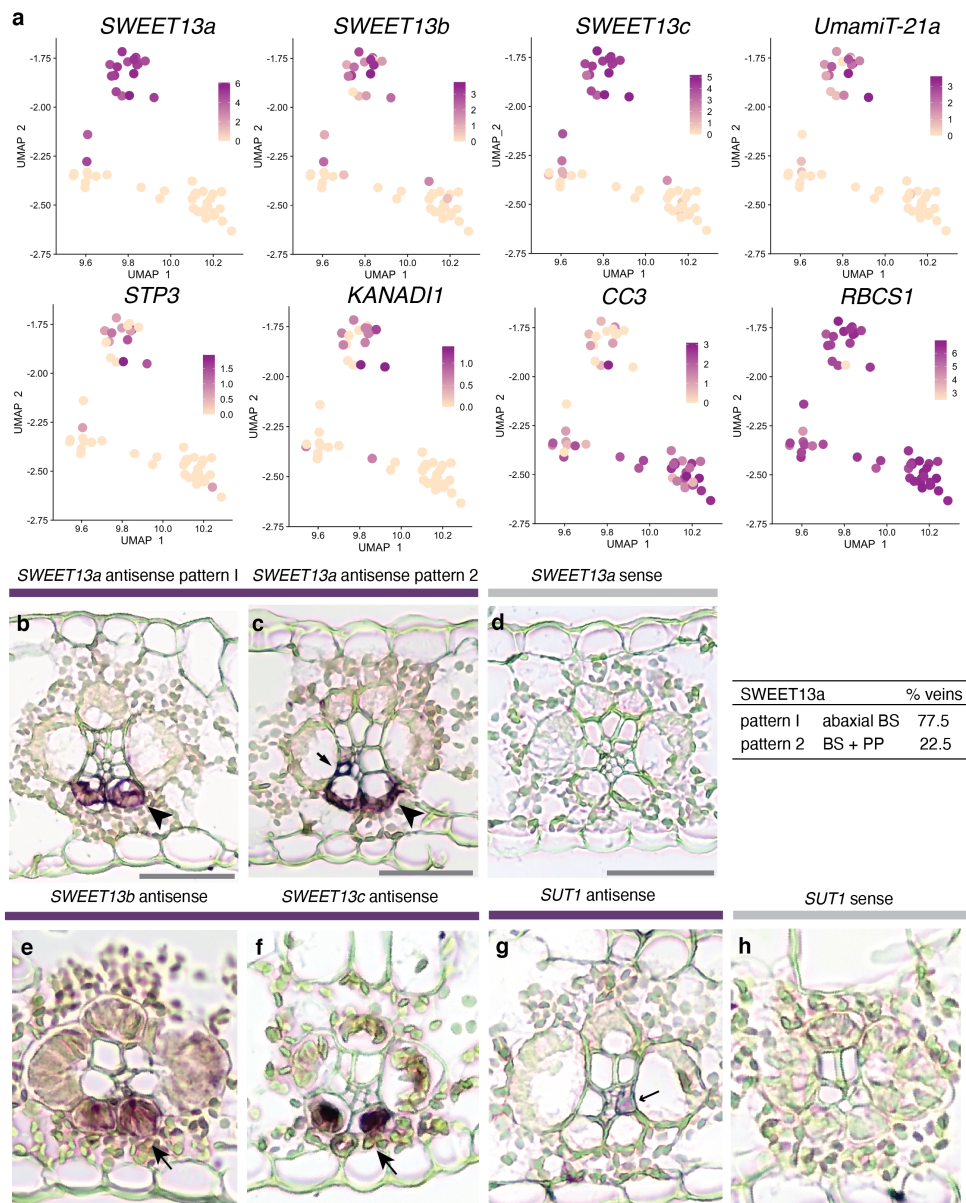
Figure 2. Abaxial BS cluster is enriched for genes encoding transport proteins
a. Feature plots show normalized levels of mRNAs for genes differentially expressed between the two clusters of bundle sheath cells plotted in UMAP space. **b - f.** *In situ* hybridization of *SWEET13a*, *SWEET13b*, and *SWEET13c.* Rank-2 intermediate veins from sections hybridized with antisense probes for *SWEET13a*, *SWEET13b*, and *SWEET13c* showed mRNA localization of three SWEET13 genes was largely limited to abaxial bundle sheath cells. **b - c.** *SWEET13a* mRNA localization was predominantly in [ab]BS cells in the majority of veins (77.5%) and to PP in a subset of veins (22.5%) (n = 824). **d.** No staining was visible after hybridization with *SWEET13a* sense probe. **e – f.** *SWEET13b* and *SWEET13c* probes showed signal predominantly in [ab]BS cells. **g.** *SUT1* mRNA is localized to a vascular cell which is likely a companion cell in rank-2 intermediate veins (arrow). **h.** No staining visible after hybridization with *SUT1* sense probe. See Supplementary Figure 5 for intermediate rank-1 and major veins. All error bars are 100μm.
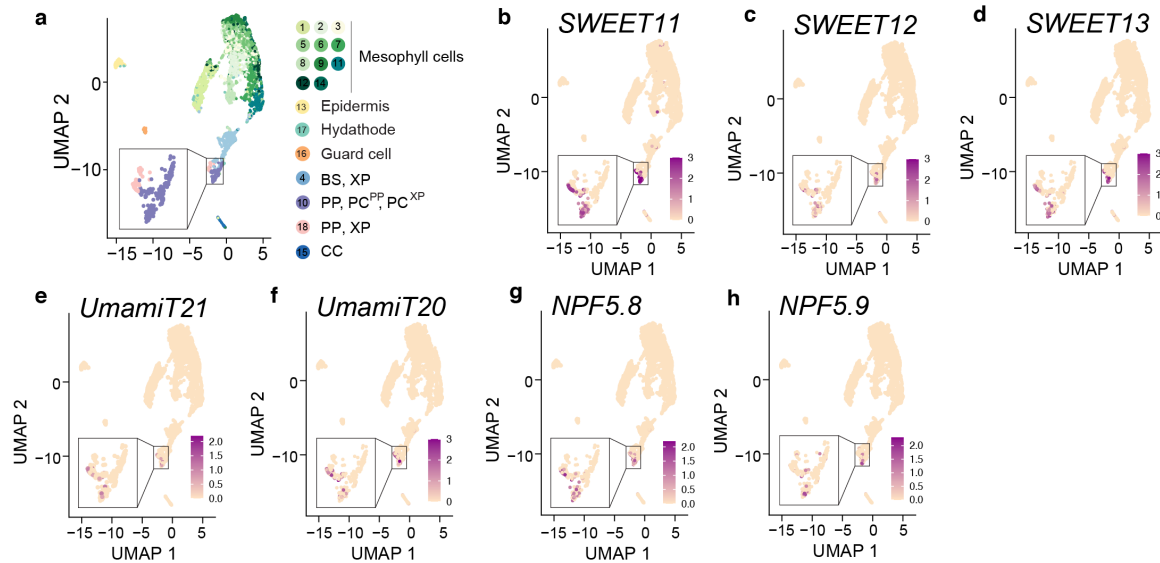
Figure 3.

Figure 3. Arabidopsis homologs of maize abBS-specific genes are expressed in Arabidopsis phloem parenchyma

Maize transporters showing abBS mRNA enrichment are homologous to many Arabidopsis transporters with Arabidopsis phloem parenchyma mRNA enrichment. **a.** UMAP plot showing 2D representation of cell relationships in multidimensional space for single-cell sequencing of Arabidopsis leaf. Clusters are indicated by colors to the right of the UMAP plot. Feature plots show normalized levels of mRNA transcripts for Arabidopsis transport proteins homologous to abBS transport proteins. **b-d.** *AtSWEET11* (AT3G48740), *12* (AT5G23660), and *13* (AT5G50800) are orthologs to *ZmSWEET13a*, *b*, and *c*. **e.** *AtUmamiT21* (AT5G64700) is homologous to *ZmUmamiT21a*. **f.** *AtUmamiT20* (AT4G08290) is homologous to *ZmUmamiT21a* (Supplementary Fig. 4). g-h. *AtNPF5.8* (AT5G14940)_and *AtNPF5.9* (AT3G01350) are homologous to *ZmNRT1*.
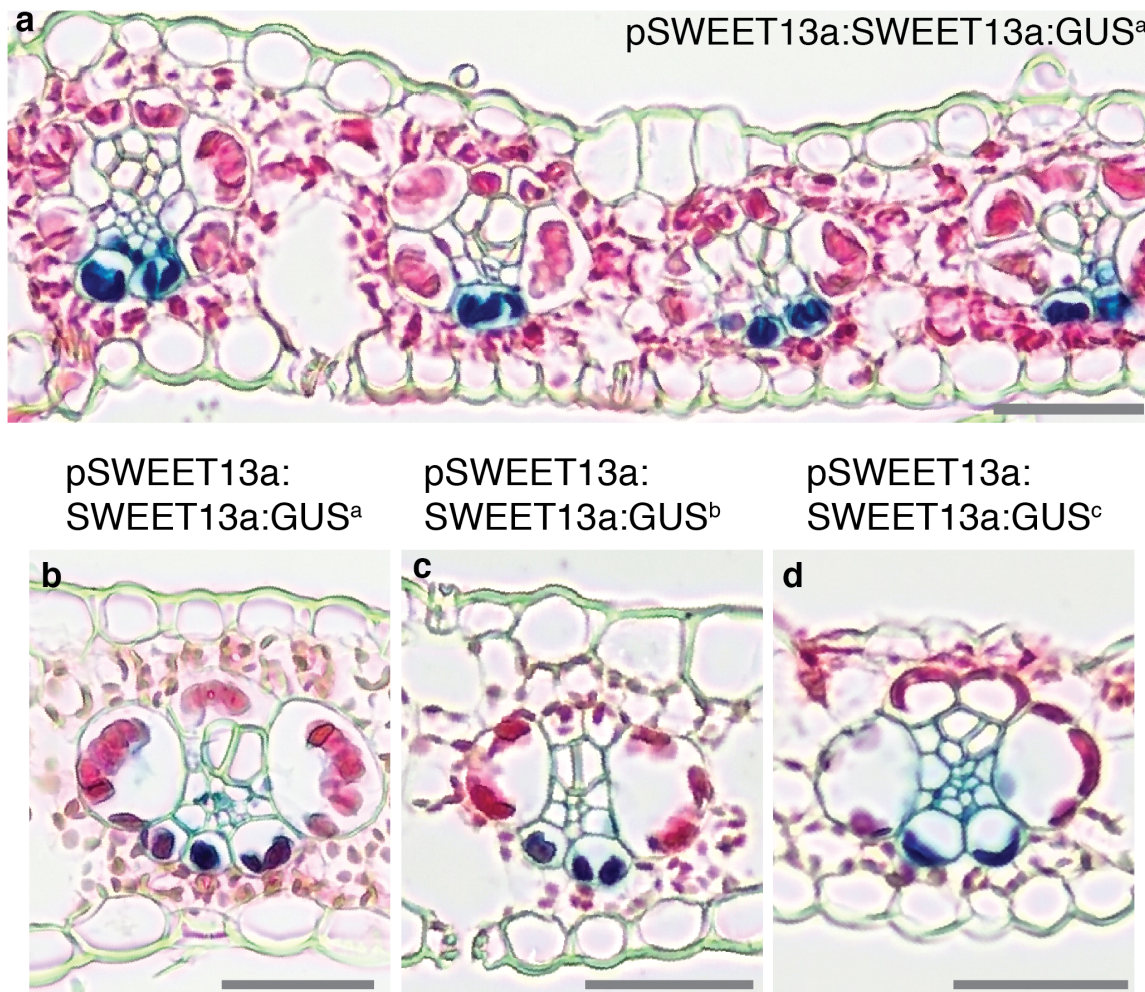
Figure 4.

Figure 4. SWEET13a protein is localized to abaxial BSC of rank-2 veins
GUS histochemistry in leaves of maize lines transformed with the translational fusion construct pSWEET13a:SWEET13a-GUS. **a.** Chloro-bromoindigo precipitate (blue) is detected specifically in abaxial bundle sheath cells of maize plants transformed with pSWEET13a:SWEET13a:GUSplus. **b - d**. Three independent transformation events (a, b, and c: pSWEET13a:SWEET13a:GUS[a, b,] and [c]) showed similar expression patterns in rank-2 intermediate veins, rank-1 intermediate veins, and major veins (for rank-1 and major veins see Supplementary Fig. 5). **b.** Line "a," **c.** Line "b," **d.** Line "c." Sections are counterstained with Eosin-Y; scale bars are 100 μm.

Figure 5.
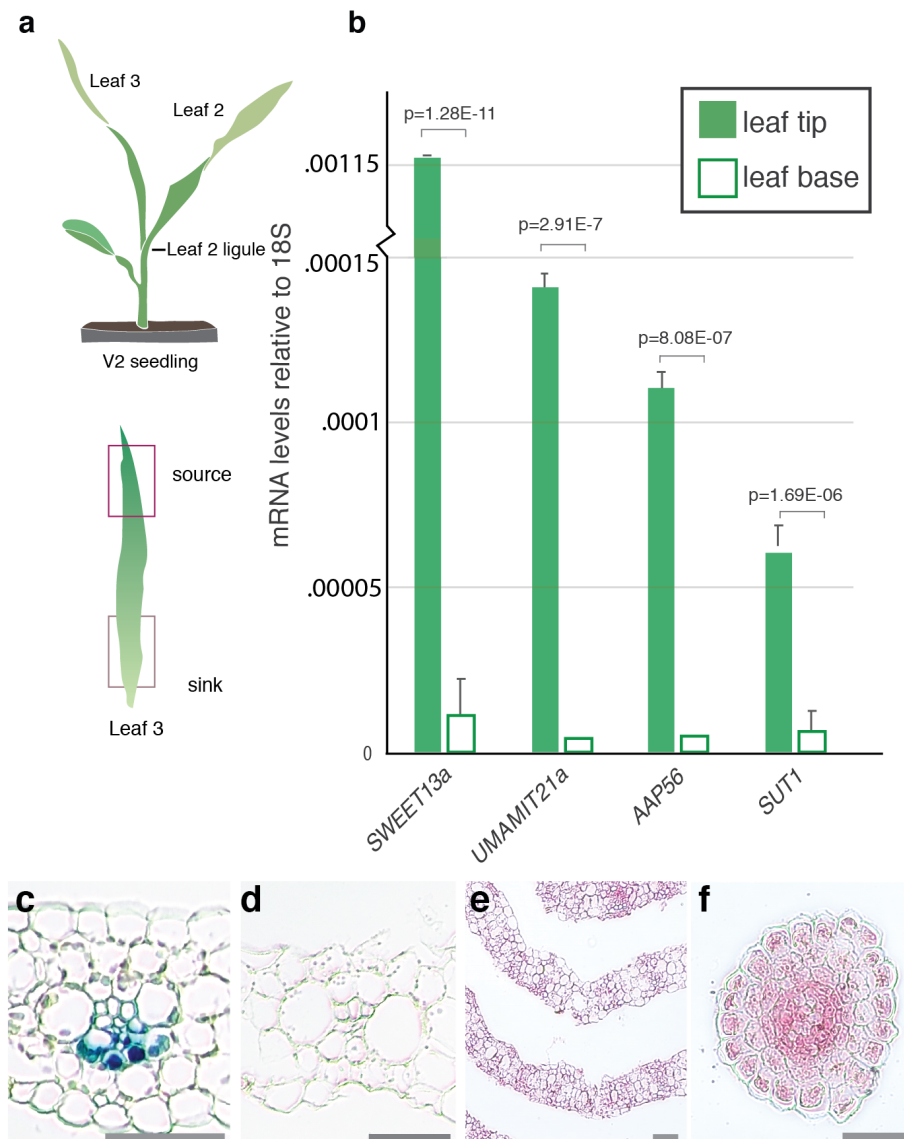
Figure 5. Abaxial BS transcripts are co-regulated during the sink-source transition

a. Tissue selected for qRT-PCR: V2-stage seedling with source and sink tissue highlighted; base of leaf 3 is still in the whorl and is net-sink tissue (Li et al., 2010). **b.** 18S-normalized mRNA levels of [ab]BS-specific transport proteins (*SWEET13a*, *UmamiT21a*, *AAP45*) and *SUT1* in source (tip) and sink (base) tissue. Values are average of three technical (qRT-PCR) replicates of three pools of two plants; error bars represent SEM. *Students two-tailed paired t-test values shown. Independent repeats confirmed the data.
c. pSWEET13a:SWEET13a:GUSplus transformed B73 seedling segments after 12-48 h incubation in GUS staining solution. V2 leaf 3 tip (12 h), **d.** leaf 3 sheath (48 h), **e.** stem cross section 1 cm above soil (48 h), **f.** cross section across root tip (48 h), Of these, only the tip of leaf 3 (source) showed chloro-bromoindigo precipitate indicative of SWEET13a expression. Scale bars: 100 μm.
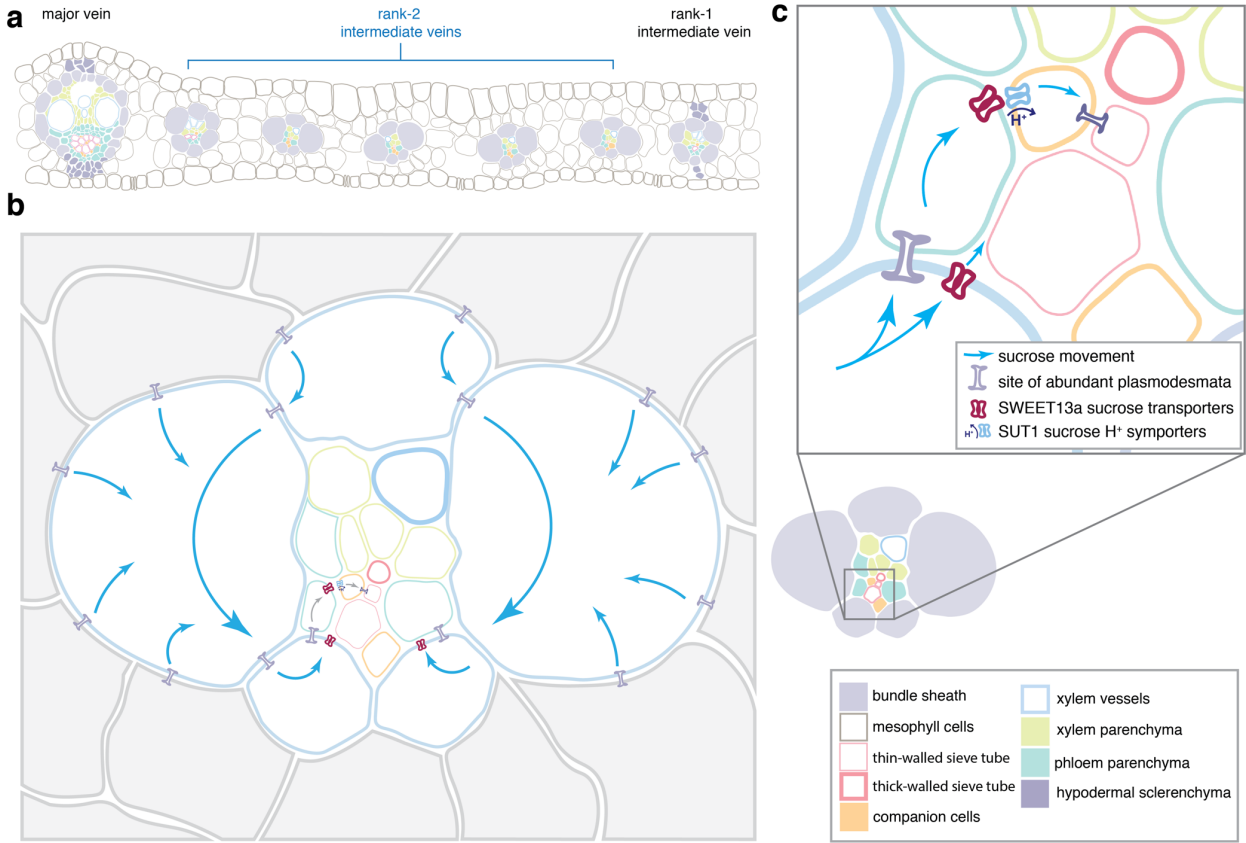
38

**Figure 6. Phloem loading occurs via the [ab]BS in maize**
a. Example of arrangement and relative numbers of major veins, rank-1 intermediate veins, and rank-2 intermediate veins in a mature maize leaf. Note that rank-1 intermediate veins are distinguished from rank-2 by the presence of hypodermal sclerenchyma. **b.** A rank-2 intermediate vein surrounded by bundle sheath (blue outline) and mesophyll (grey) cells. Sucrose movement down its concentration gradient is indicated by blue arrows. **b.** Inset panel shows detail of sucrose movement from bundle sheath cells into apoplasm via SWEET13 transporters, or to phloem parenchyma (teal) via plasmodesmata, where it is then effluxed to the apoplasmic space by SWEETs. Sucrose in the apoplasm is taken up by SUT1 into the companion cells-sieve element (orange, pink) complex for long distance transport.

SUPPLEMENTARY DATA

Supplementary text

**A subset of mesophyll cells appears to be specialized in iron metabolism**

Subcluster MS5 (visible in the lower left corner of Figure 1b) shared mesophyll identity but appeared be specialized in metal accumulation and transport, as indicated by high and specific expression of four nicotianamine synthase genes, *NAS1, 2,* 9, and *10*, which are involved in iron chelation; one iron phytosiderophore transporter. *YS1* (*yellow stripe 1*); and various additional genes involved in metal transport and metabolism (Supplementary Table 1). M5 cells could either represent a cell type with a specific localization in the leaf or correspond to cells that contain different levels of iron.
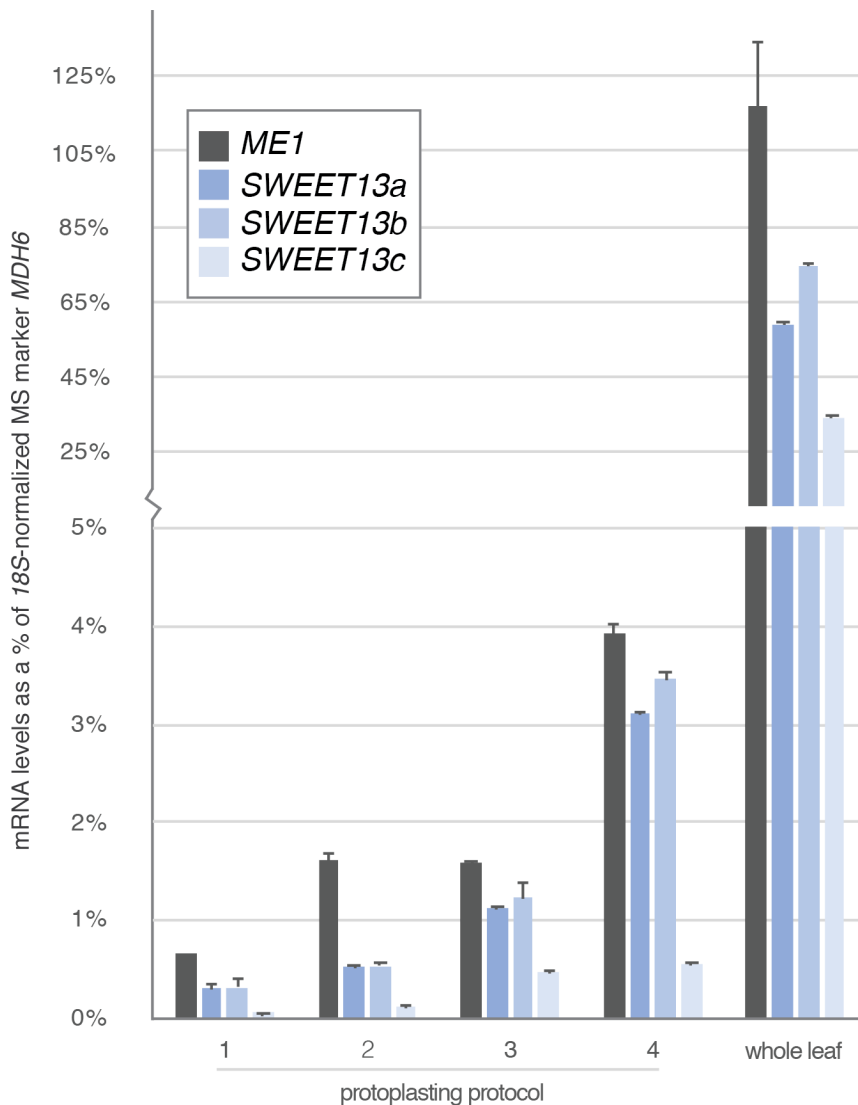
Supplementary Figure 1. qRT-PCR of putative BSC and vascular-expressed genes as an indication of protoplast cell type diversity prior to sequencing

Normalized mRNA levels of *ME1*, *SWEET13a*, *SWEET13b*, and *SWEET13c* shown as a percentage of *18S*-normalized expression of a mesophyll marker gene, *NADP-malate dehydrogenase6* (*MDH6*), after different protoplasting treatments. Error bars represent SEM of technical duplicates.

Protocol 1, standard enzyme cocktail (see Materials and Methods) with 3.5 h incubation. Protocol 2, doubled enzyme concentration. Protocol 3, isolated BS strands released after 2 h and continued protoplasting of filtered BS strands in fresh enzyme solution to deplete mesophyll cells. Protocol 4, incubated leaf tissue in pretreatment solution (2 mM L-cysteine and 164 mM sorbitol), which yielded the highest ratio of BS:MS marker genes.
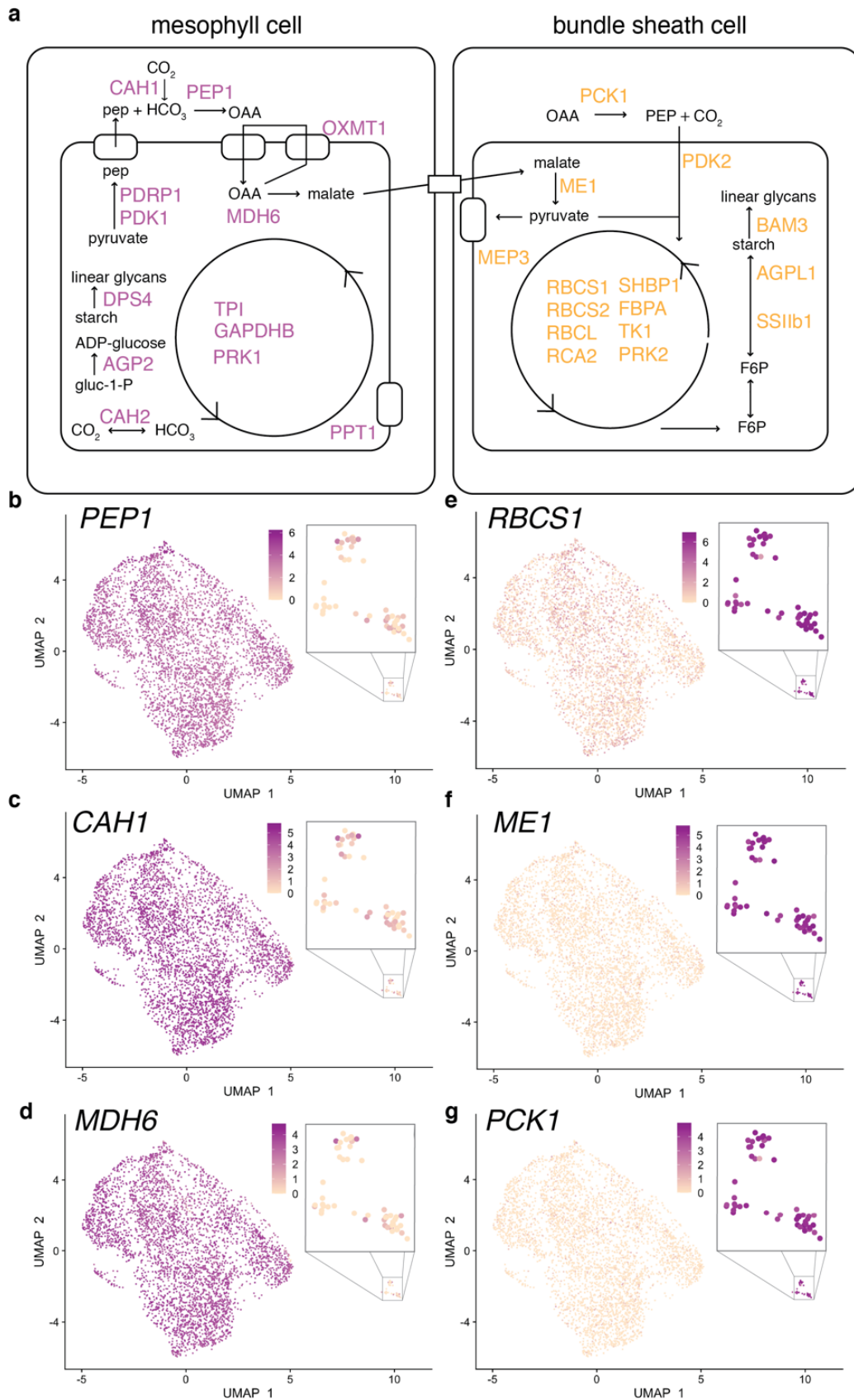
Supplementary Figure 2. Schematic of C4 photosynthesis related genes and relative expression in BS and MS clusters.

a. Partitioning of proteins involved in C4 photosynthesis between mesophyll and bundle sheath cells in maize(Friso et al., 2010). For all proteins displayed, mRNA expression in this scRNA-seq dataset was specific to either mesophyll or bundle sheath cells (logFC > 1.0; FDR-adjusted p-value < .05). **b**. Gene IDs, symbols, and full names are shown along with Log FC values in Supplementary Table 2. **b-g.** Feature plots show normalized levels of mRNAs for canonical C4 photosynthesis genes expressed differentially in mesophyll and bundle sheath. **b.** *PEP1* (Phosphoenolpyruvate carboxylase 1; Zm00001d046170) **c.** *CAH1* (Carbonic anhydrase 1; Zm00001d044099) **d.** *MDH6* (NADP-dependent malate dehydrogenase 6; Zm00001d031899) **e.** *RBCS1* (Ribulose bisphosphate carboxylase small subunit 1; Zm00001d052595) **f.** *ME1* (NADP-dependent malic enzyme 1; Zm00001d000316) **g.** *PCK1* (Phosphoenolpyruvate carboxykinase 1; Zm00001d028471)
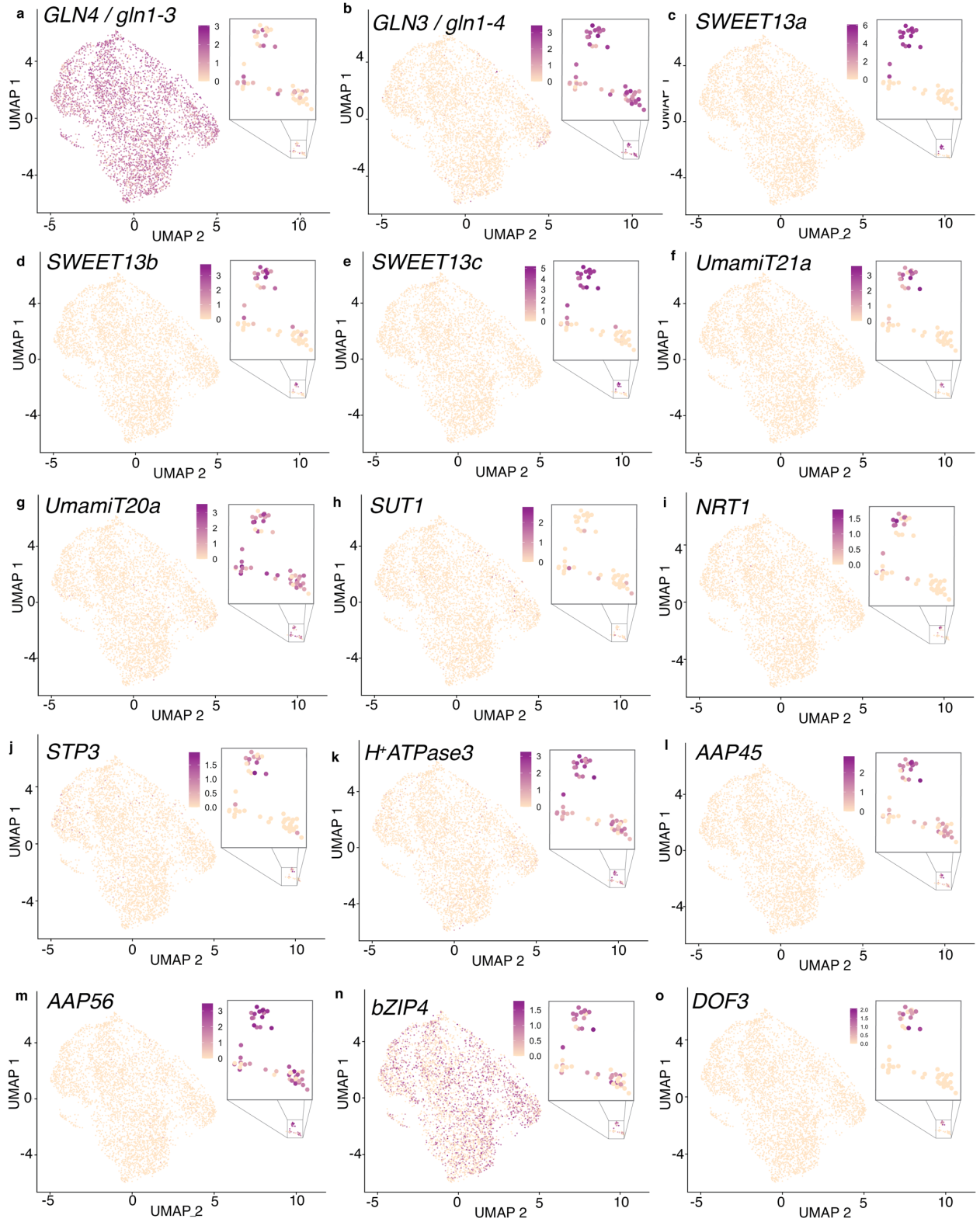
Supplementary Figure 3. UMAP plots of glutamine synthetase, transport-related proteins, and transcription factors in bundle sheath cells
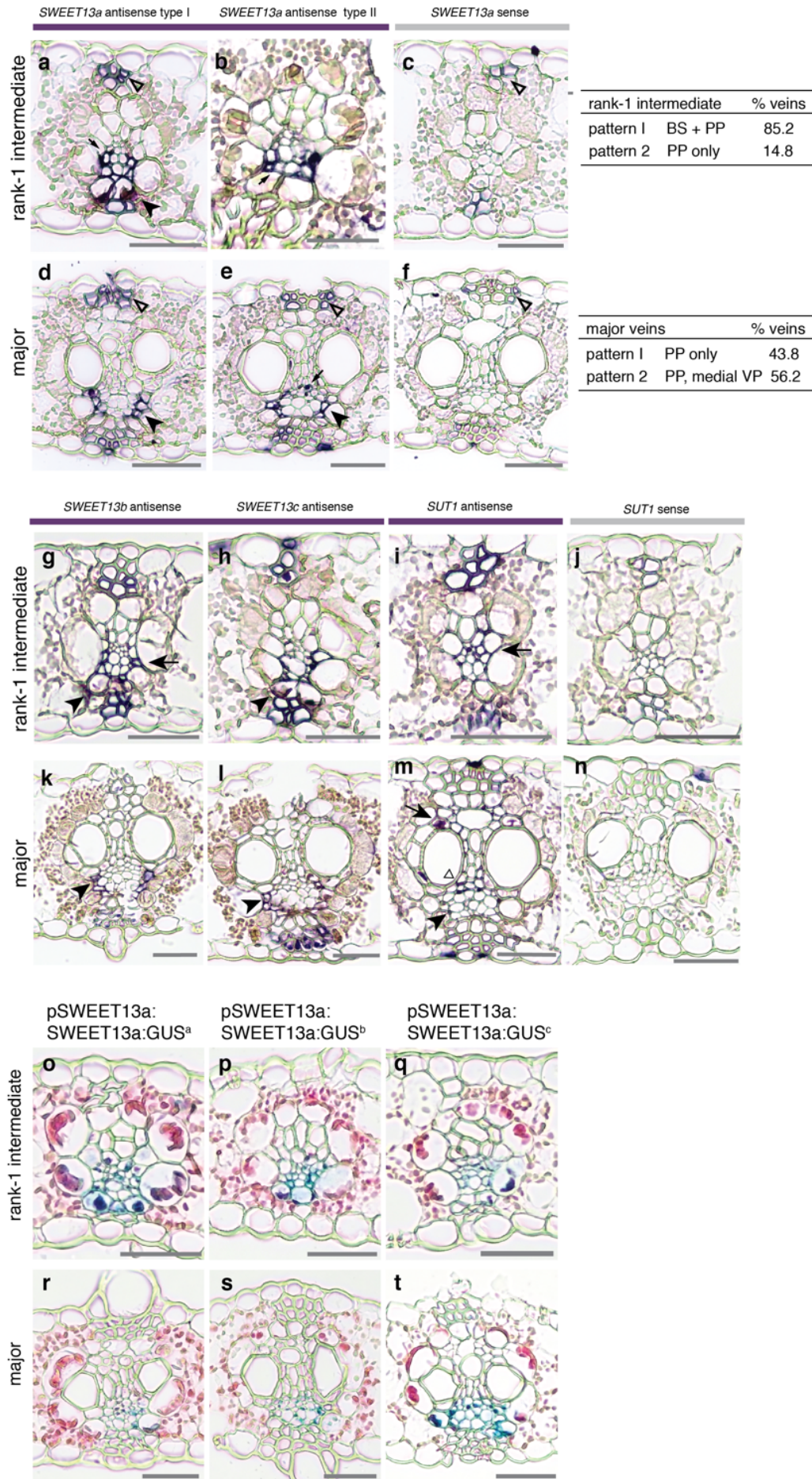
a - b. Feature plots show normalized levels of mRNA transcripts for glutamine synthetase genes expressed differentially in mesophyll and bundle sheath. **a.** *GLN4 (gln1-3*, protein GS3, Zm00001d017958) is widely expressed in mesophyll cells and some bundle sheath cells. **b.** *GLN3 (gln1-4*, protein GS4, Zm00001d028260) is expressed in bundle sheath cells.

c – o. Feature plots show normalized levels of mRNA transcripts for transport-related genes and transcription factors expressed in ^{ad}BS or ^{ab}BS. **c.** *SWEET13a* (Zm00001d023677), **d.** *SWEET13b* (Zm00001d023673), **e.** *SWEET13c* (Zm00001d041067), and **f.** *UmamiT21a* (Zm00001d035717) are specific to ^{ab}BS. **g.** *UmamiT20a* (Zm00001d044951) is expressed in ^{ab}BS and ^{ad}BS. **h.** *SUT1* (Zm00001d027854) is not highly expressed in any cell type in this dataset. **i.** *NRT1* (Zm00001d044768), **j.** *STP3* (Zm00001d027268), **k.** *H$^+$ATPase3* (Zm00001d019062)*,* **l.** *AAP45* (Zm00001d035243), **m.** *AAP56* (Zm00001d012231), **n.** *bZIP4* (Zm00001d018178) and **o.** *DOF3* (Zm00001d035651) are enriched in ^{ab}BS relative to ^{ad}BS.
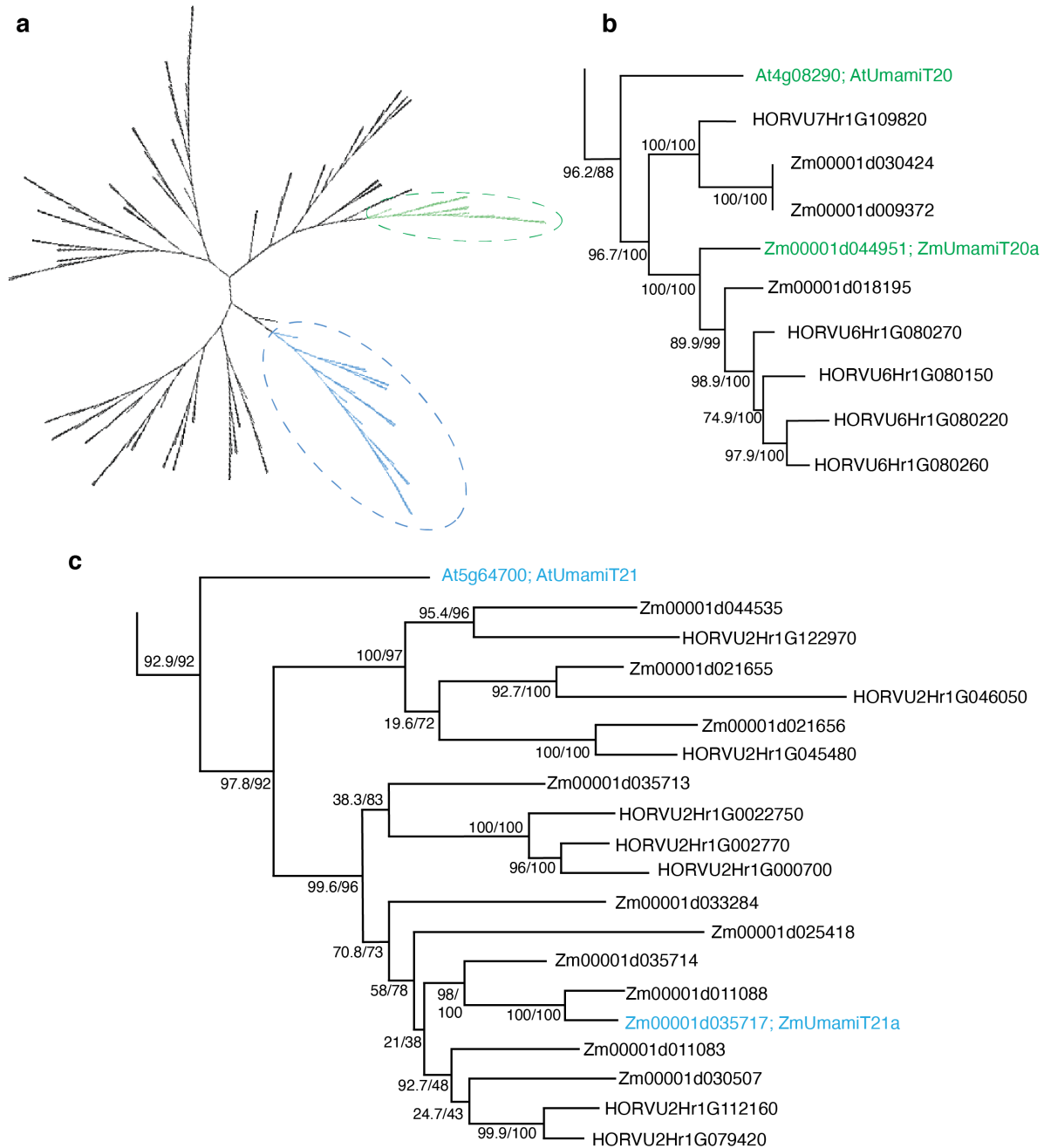
Supplementary Figure 4. Neighbor joining tree of family of UmamiT amino acid transporters in Arabidopsis, maize, and barley

a. Cladogram of all UmamiT amino acid sequences in maize, barley, and Arabidopsis **b.** Phylogram of green highlighted clade containing the ZmUmamiT expressed in all BSC types. Zm00001d44951 is most closely related to Arabidopsis UmamiT20. **c.** Phylogram of blue highlighted clade containing the ZmUmamiT expressed specifically in [ab]BSC. Zm00001d035717 is most closely related to Arabidopsis UmamiT21. Values at nodes are % UF-bootstraps out of 1000/% SH-aLRT.

| rank-1 intermediate		% veins
pattern I	BS + PP	85.2
pattern 2	PP only	14.8

major veins		% veins
pattern I	PP only	43.8
pattern 2	PP, medial VP	56.2

Supplementary Figure 5. SWEET and SUT mRNA localization and SWEET13a protein localization in rank-2 intermediate and major veins

a - c. SWEET13a mRNA localization in rank-1 intermediate veins **a.** Pattern 1: [ab]BSC (arrowhead) and vascular parenchyma (VP) (arrow), and **b.** Pattern 2: mainly in VP (arrow). **c.** rank-1 vein in sense-probe-hybridized section. **d-f.** SWEET13a mRNA localization in major veins **d.** Pattern 1: in phloem parenchyma (PP) only (arrow), and **e.** Pattern 2: in PP and medial VP (parenchyma between xylem and phloem) (arrow). **f.** *SWEET13a* major vein in sense-probe -hybridized section. Hypodermal sclerenchyma is considered background (open triangles). Table indicates percentage of veins meeting the above criteria for each vein type. Rank-1 intermediate, n = 196; and major veins, n = 98; variable n-numbers are due to relative proportions of each vein type in the leaf. Scale bars are 100 µm.

g - j. *SWEET13b*, *c*, and *SUT1* mRNA localization in rank-1 intermediate veins. **g.** For *SWEET13b* antisense probe-hybridized rank-1 intermediate veins, staining was in [ab]BS (arrowhead) and vascular parenchyma (arrow). **h.** For *SWEET13c* antisense probe-hybridized rank-1 intermediate veins, staining was in [ab]BS (arrowhead) and vascular parenchyma (arrow). **i.** For *SUT1* antisense probe-hybridized rank-1 intermediate veins, staining was in vasculature (arrow). **j.** *SUT1* sense probe-hybridized rank-1 intermediate vein.

k - n. *SWEET13b*, *c*, and *SUT1* mRNA localization in major veins. **k.** For *SWEET13b* antisense probe-hybridized major veins, staining was in phloem parenchyma (arrowhead). **l.** For *SWEET13c* antisense probe-hybridized major veins, staining was in phloem parenchyma (arrowhead). **m.** For *SUT1* antisense probe-hybridized major veins, staining was in companion cells (arrow), in vascular parenchyma between xylem and phloem (triangle), and in xylem parenchyma (arrowhead). **n.** *SUT1* sense probe-hybridized major vein. Scale bars are 100 µm.

o – t. SWEET13a protein localization as visualized by GUS staining of SWEET13a:GUS-transformed B104 plants . Chloro bromoindigo precipitate is localized to abaxial portion of veins in both rank-1 intermediate (**o – q**) and major veins (**r – t**) of all three independent transformation events. Scale bars are 100 µm; sections are counterstained with Eosin-Y.

48
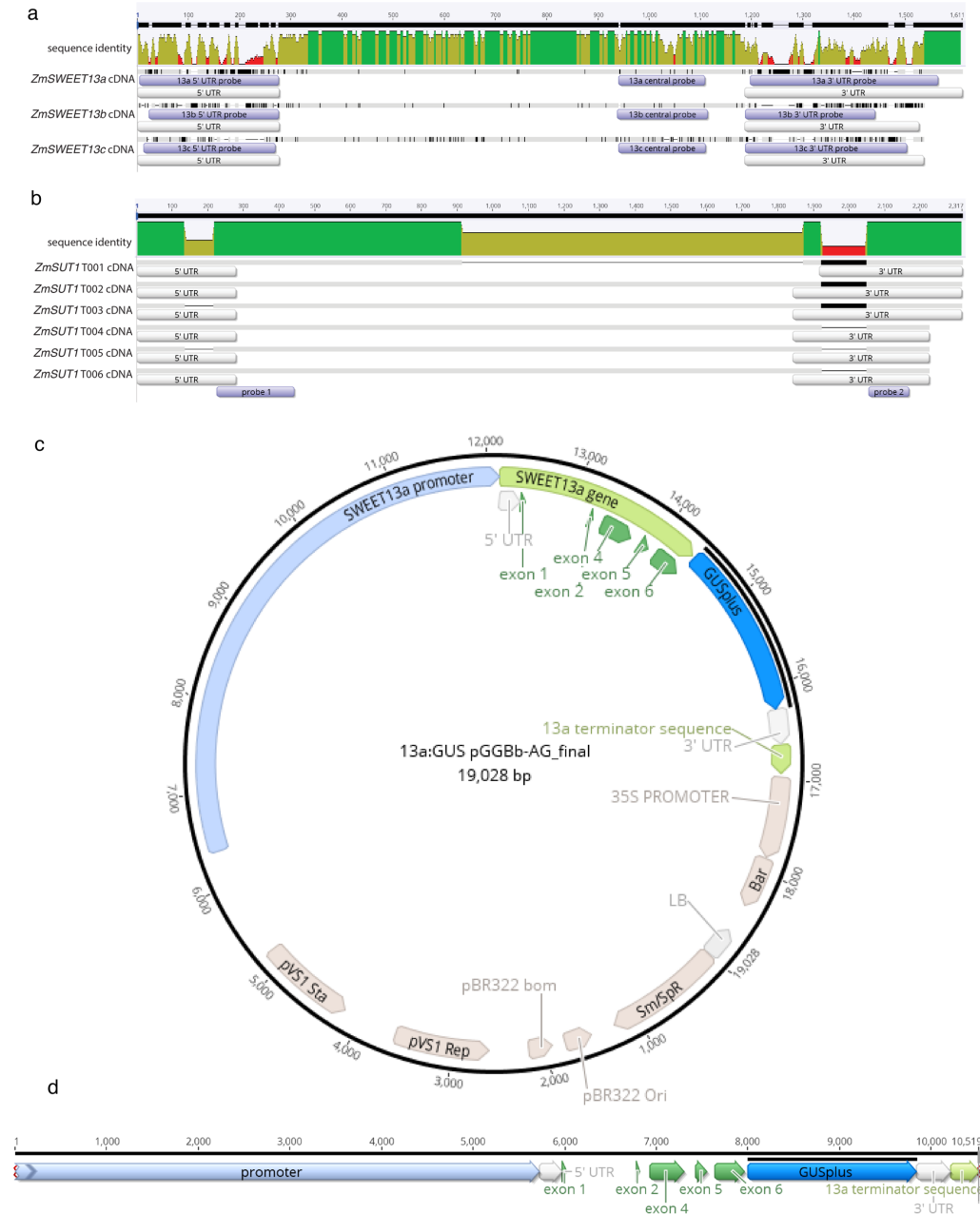
Supplementary Figure 6. Probe design for in situ hybridization and pSWEET13a:SWEET13a:GUS construct schematic

a. *ZmSWEET13a*, *b*, and *c* aligned using MUSCLE in Geneious. Regions used as templates for RNA probes are highlighted in purple. Three probes in unique regions of each gene allowed us to differentiate between the homologs. **b.** The six isoforms of *ZmSUT1* aligned using MUSCLE in Geneious; two regions common to all six isoforms were selected for probe templates. Two unique regions in ZmUMAMIT21a and ZmME1 were selected for probe templates.**c.** Circular schematic of plasmid used to transform B104. The construct included the 5751 bp upstream of the start codon (lavender), all exons and introns of the SWEET13a gene (green), a 9-alanine linker fused to GUSplus (blue), followed by 684 bp downstream of stop codon (green). d. linear schematic of the SWEET13a:GUS construct

49
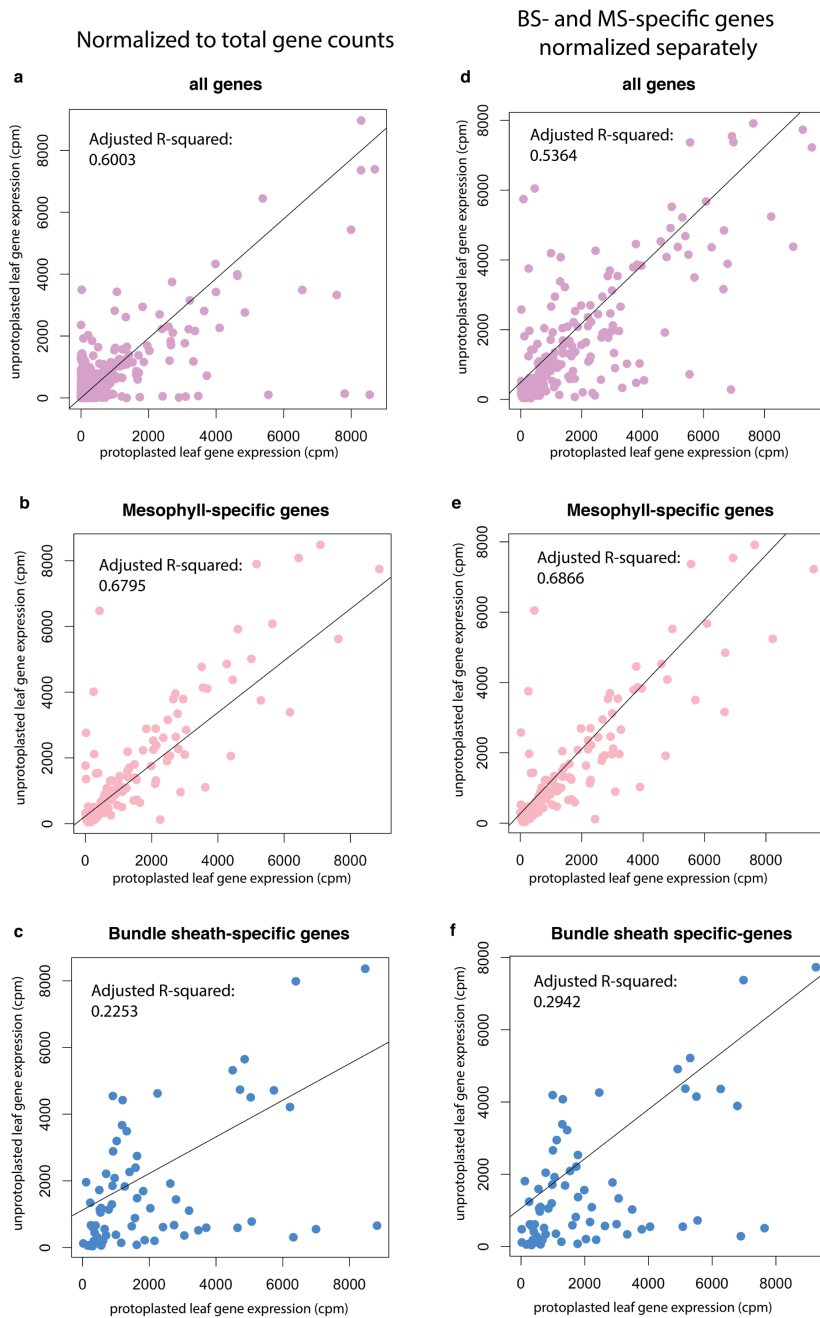
Supplementary Figure 7. Correlation of mRNA counts between protoplasted cells and whole leaf

a. mRNA counts in whole leaf and protoplasted leaf expressed as counts per million reads (cpm) with adjusted R-squared values. **b**. mRNA counts for mesophyll cell-specific genes, as determined by unsupervised marker gene discovery (see materials and methods). **c.** mRNA counts for bundle sheath-specific genes. In **d-f**: counts of MS- and BS-specific genes were normalized separately to compensate for differing ratios of cell types represented in bulk leaf and protoplast samples. **d.** MS- and BS-specific genes, normalized separately. **e.** MS-specific genes normalized to total counts of MS-specific genes. **f.** BS-specific genes normalized to total counts of BS-specific genes. TMM method of normalization.

Supplementary Table 2. mRNA enrichment of C4 photosynthesis-related genes in MS and BS clusters

mesophyll	Symbol or abbreviation	Log FC	Gene name
Zm00001d031899	*MDH6*	3.00	NADP-dependent malate dehydrogenase 6
Zm00001d046170	*PEP1*	3.20	Phosphoenolpyruvate carboxylase 1
Zm00001d044099	*CAH1*	3.58	Carbonic anhydrase 1
Zm00001d011454	*CAH6*	3.58	Carbonic anhydrase 6 (chloroplast localized)
Zm00001d023929	*OXMT1*	1.50	Oxo-glutarate/malate transporter1 (OMT)
Zm00001d038163	*PDK*	1.45	Pyruvate, phosphate dikinase 1
Zm00001d006520	*PDRP1*	2.95	Pyruvate, phosphate dikinase regulatory protein 1
Zm00001d032383	*PPT1*	0.99	Phosphate/phosphoenolpyruvate translocator 1
Zm00001d035737	*PRK1*	2.18	D-glycerate 3-kinase chloroplastic
Zm00001d027488	*GAPB1*	2.10	Glyceraldehyde phosphate dehydrogenase B1
Zm00001d021310	*TPI*	2.54	Triosephosphate isomerase
Zm00001d039131	*AGP2*	0.86	ADP glucose pyrophosphorylase 2
Zm00001d027309	*DPS4*	n/a	Phosphoglucan phosphatase DSP4 chloroplastic

bundle sheath	Symbol or abbreviation	Log FC	Gene name
Zm00001d004894	*RBCS2*	5.19	Ribulose biphosphate carboxylase small subunit 2
Zm00001d052595	*RBCS1*	5.18	Ribulose biphosphate carboxylase small subunit 1
Zm00001d006402	*RBCL*	2.08	Rubisco large chain (genomic, introns)
Zm00001d028471	*PCK1*	4.23	Phosphoenolpyruvate carboxykinase 1
Zm00001d000316	*ME1*	5.04	NADP-dependent malic enzyme
Zm00001d045451	*TK1*	2.20	Transketolase 1
Zm00001d010321	*PDK2*	1.58	Pyruvate orthophosphate dikinase 2
Zm00001d042050	*MEP3*	3.78	Protein RETICULATA-RELATED 4
Zm00001d000164	*PRK2*	1.14	Phosphoribulokinase chloroplastic 4
Zm00001d048593	*RCA2*	3.79	Rubisco activase 2
Zm00001d023559	*FBPA*	5.31	Fructose-bisphosphate aldolase
Zm00001d053015	*FBPA*	2.89	Fructose-bisphosphate aldolase
Zm00001d042840	*SHBP1*	3.78	Sedoheptulose-17-bisphosphatase 3 chloroplastic
Zm00001d018936	*RPE*	3.67	Probable ribose-5-phosphate isomerase 3 chloroplastic
Zm00001d033910	*AGPL1*	2.14	ADP glucose pyrophosphorylase large subunit leaf 1
Zm00001d047077	*BAM3*	1.09	Beta-amylase 3
Zm00001d026337	*SSIII1b*	0.60	Starch synthase IIIb-1

Supplementary Table 4. Genes used in this study

AGPv4 ID	gene	full name
Zm00001d023677	SWEET13a	SWEET13a
Zm00001d023673	SWEET3b	SWEET13b
Zm00001d041067	SWEET13c	SWEET13c
Zm00001d027854	SUT1	Sucrose Transporter 1
Zm00001d048611	MT1b	Metallothionein-like protein 1B
Zm00001d038558	CC3	Cystatin3
Zm00001d004894	RBCS2	ribulose bisphosphate carboxylase small subunit2
Zm00001d052595	RBCS1	ribulose bisphosphate carboxylase small subunit1
Zm00001d000316	ME1	NADP-dependent malic enzyme
Zm00001d053281	NAAT1	Nicotianamine aminotransferase
Zm00001d016441	TAAT	Tyrosine aminotransferase
Zm00001d044099	CAH1	Carbonic anhydrase 1
Zm00001d031899	MD6	NADP-dependent malate dehydrogenase 6
Zm00001d046170	PEP1	Phosphoenolpyruvate carboxylase 1
Zm00001d028471	PCK1	Phosphoenolpyruvate carboxykinase 1
Zm00001d047658	NAS10	Nicotianamine synthase10
Zm00001d047651	NAS1	Nicotianamine synthase 1
Zm00001d028887	NAS9	Nicotianamine synthase 9
Zm00001d028888	NAS2	Nicotianamine synthase2
Zm00001d017429	YS1	Iron-phytosiderophore transporter yellow stripe 1
Zm00001d033496	Nas3	Nicotianamine synthase 3
Zm00001d035243	AAAP45	Amino acid permease 45
Zm00001d012231	AAAP56	Amino acid permease 56
Zm00001d035717	UmamiT21a	UmamiT21a
Zm00001d044951	UmamiT20a	UmamiT20a
Zm00001d010321	PDK2	Pyruvate orthophosphate dikinase 2
Zm00001d038163	PDK1	Pyruvate orthophosphate dikinase1
Zm00001d031899	MDH6	NADP-dependent malate dehydrogenase 6
Zm00001d017958	GLN4	glutamine synthetase 4 (gln1-3)
Zm00001d033747	GLN2	glutamine synthetase 2 / Glutamine synthetase root isozyme 2
Zm00001d026501	GLN1	glutamine synthetase 1 leaf isozyme chloroplastic
Zm00001d028260	GLN3	glutamine synthetase 3 / 6 / root isozyme 5 (gln1-4)
Zm00001d044768	NRT1	Protein NRT1/ PTR FAMILY 5.8
Zm00001d027268	STP3	Sugar transport protein 3
Zm00001d019062	H+ATPase	membrane H(+)-ATPase3
Zm00001d018178	bZIP4	basic leucine zipper 4 / ABA-insensitive 5-like protein
Zm00001d010201	MYB25	Transcription repressor MYB6 / myb25